Technische Universiteit Delft

Distant Retrograde Orbits

AE4020: Literature Study

Dominik M. Stahl

TU Delft

Distant Retrograde Orbits

AE4020: Literature Study

by

Dominik M. Stahl

Submitted in partial fulfilment of the requirements
for the Degree of Master of Science (MSc) in Aerospace Engineering
at Delft University of Technology

Student number: 5144825
Project duration: September 22 – November 26, 2020
Supervisor: Ir. Ron Noomen

Contents

List of Abbreviations

ABM	Adams-Bashforth-Moulton (Method)
BS	Buliersch-Stoer (Method)
CR3BP	Circular Restricted Three-Body Problem
CW	Clohessy-Wiltshire
DOPRI	Dormand-Prince (Method)
DRO	Distant Retrograde Orbit
GA	Genetic Algorithm
JSON	JavaScript Object Notation
LEO	Low Earth Orbit
LLO	Low Lunar Orbit
MEE	Modified Equinoctial Elements
n.c.	normalized coordinates
p.m.g.	Point Mass Gravity
PSO	Particle Swarm Optimization
RAAN	Right Ascension of the Ascending Node
RK	Runge-Kutta (Method)
RK4	Fourth-Order Runge-Kutta Method
RKF	Runge-Kutta-Fehlberg (Method)
S/C	Spacecraft
s.h.g.	Spherical Harmonics Gravity
s.r.p.	Solar Radiation Pressure
Tudat	TU Delft Astrodynamic Toolbox
USM	Unified State Model
WP	Work Package

List of Symbols

Latin Symbols

A	Lindstedt Series Parameter	[-]
a	Semi-Major Axis	[m]
$\mathbf{a}_{\text{(pert)}}$	(Perturbation) Acceleration Vector	[m/s^2]
a_{lm}	Spherical Harmonics Gravity Field Acceleration	[m/s^2]
a_n	Fourier Series Parameter	[-] (n.c.)
$a_{n,l}$	Runge-Kutta Method Parameter	[-]
B	Lindstedt Series Parameter	[-]
b	Lindstedt Series Coordinate	[-]
b_n	Fourier Series Parameter	[-] (n.c.)
b_n	Runge-Kutta Method Parameter	[-]
C	Lindstedt Series Parameter	[-]
C	Jacobi Constant in CR3BP	[-]
$\bar{C}_{lm}$	Normalized Spherical Harmonics Gravity Field Coefficient	[-]
$\mathbf{c_1}$, $\mathbf{c_2}$	Coordinates of Primary and Secondary	[-] (n.c.)
c_n	Runge-Kutta Method Parameter	[-]
D	Lindstedt Series Parameter	[-]
E	Eccentric Anomaly	[rad]
e	Eccentricity	[-]
$\mathcal{F}$	Auxiliary Function for Encke Propagator	[-]
F	Force	[kg m/s^2]
$\mathbf{F}$	Force Vector	[kg m/s^2]
f	Modified Equinoctial Elements Parameter	[-]
$\mathbf{f}$, f	General Function for First-Order Differential Equation	*depends on application*
G	Universal Gravitational Constant	[m^3/kg s^2]
g	Modified Equinoctial Elements Parameter	[-]
$\mathcal{H}$	Hamiltonian	*depends on application*
h	Modified Equinoctial Elements Parameter	[-]
$\mathbf{I}$	Identity Matrix	[-]
I	Modified Equinoctial Elements Parameter	[-]
i	Inclination	[rad]
k	Spring Stiffness	[kg/s^2]
k	Constant for Lindstedt Series	[-]
k	Modified Equinoctial Elements Parameter	[-]
$\mathbf{k}_n$	Function Evaluations for Runge-Kutta Method	*depends on application*
$\mathcal{L}$	Lagrangian	*depends on application*
L	Modified Equinoctial Elements Parameter	[-]
l	Order of Spherical Harmonics	[-]
M	Set of Parameters for Nelder-Mead Algorithm	*depends on application*
M	Mean Anomaly	[rad]
$\mathbf{M}$	Monodromy Matrix	[-]
m	Mass	[kg]
m	Order of Spherical Harmonics	[-]
m_1, m_2, m_3	Masses of Bodies 1, 2 and 3	[kg]

$\bar{P}_{lm}$	Normalized Associated Legendre Polynomial	[-]
$P_{1/2/3/r/e/c}$	Sets of Parameters for Nelder-Mead Algorithm	*depends on application*
p	Semi-Latus Rectum	[m]
p_i	Generalized Momenta	*depends on application*
Q	Lindstedt Series Coordinate	[-]
q	Lindstedt Series Coordinate	[-]
q_i	Generalized Coordinates	*depends on application*
q	Auxiliary Variable for Encke Propagator	[-]
R	Radius of Earth	[m]
r	Distance (Between Two Bodies)	[m]
$\mathbf{r}$	Position Vector	[m]
r_1, r_2	Distance to Primary and Secondary	[-] (n.c.)
r_p	Parameter in DRO Modeling	[-] (n.c.)
$\mathbf{S}$	State Vector	*depends on application*
$\bar{S}_{lm}$	Normalized Spherical Harmonics Gravity Field Coefficient	[-]
T	(Specific) Kinetic Energy	*depends on application*
t	Time	[s] or [-] (n.c.)
U	Potential	[m^2/s^2] or [-] (n.c.)
V	(Specific) Potential Energy	*depends on application*
$\mathbf{X}$	State Vector in CR3BP	[-] (n.c.)
X	Generalized Momenta in CR3BP	[-] (n.c.)
X	Generalized Momenta in Hill Problem	[-] (n.c.)
x	Coordinates in CR3BP	[-] (n.c.)
x	Coordinates of Cowell Propagator	[m]
x	Coordinates in Hill Problem	[-] (n.c.)
Y	Generalized Momenta in CR3BP	[-] (n.c.)
Y	Generalized Momenta in Hill Problem	[-] (n.c.)
y, $\bar{y}$	True and Estimated Solution of Differential Equation	*depends on application*
y	Coordinates in CR3BP	[-] (n.c.)
y	Coordinates of Cowell Propagator	[m]
y	Coordinates in Hill Problem	[-] (n.c.)
Z	Generalized Momenta in CR3BP	[-] (n.c.)
z	Coordinates in CR3BP	[-] (n.c.)
z	Coordinates of Cowell Propagator	[m]

Greek Symbols

Γ	Jacobi Constant in Hill Problem	[-]
η	Coordinate in Hill Problem	[-] (n.c.)
θ	True Anomaly	[rad]
θ	Parameter in DRO Modeling	[rad]
θ	Angle for Spherical Harmonics	[rad]
λ_1 to λ_6	Eigenvalues of Monodromy Matrix	[-]
μ	Mass Ratio Between Primaries	[-]
μ	Standard Gravitational Parameter	[m^3/s^2]
ν	Mass Ratio Between Primaries and Third Body	[-]
ξ	Coordinate in Hill Problem	[-] (n.c.)
ρ	Distance Between Secondary and Third Body in Hill Problem	[-] (n.c.)
$\boldsymbol{\rho}$	Position on Osculating Orbit (Encke Propagator)	[m]
Φ	Potential	[-] (n.c.)
$\mathbf{\Phi}$	State Transition Matrix	[-] (n.c.)
Φ	Lindstedt Series Coordinate	[-]
ϕ	Lindstedt Series Coordinate	[-]
ϕ	Angle for Spherical Harmonics	[rad]
Ω	Right Ascension of the Ascending Node (RAAN)	[rad]
ω	Argument of Periapsis	[rad]

1 Introduction

Distant Retrograde Orbits (DROs) are orbits in which a light body – typically a spacecraft – travels about the secondary of a two-body system in reversed (retrograde) direction. This motion can be performed given that the two bodies of the two-body system orbit each other in a low eccentric way. The two-body system can be a star-planet system as for example the Sun-Earth system or a planet-moon system as the Earth-Moon system or the Jupiter-Europa system. DROs are the most stable orbits in a two-body system and therefore highly interesting for a wide range of applications: An asteroid, that is brought to the Earth-Moon system, could be placed in such an orbit and would be safely stored there for the next thousands of years. An observation mission to Jupiter's moons could benefit from the DRO's stability in order to have some close approaches with the moons. And yet, by now, a DRO has never been flown. Some remaining questions are yet to be solved regarding the modeling of and transfers to DROs.

There is no known way to describe DROs analytically. And even though there have been attempts in the past to model DROs, a good and general model has not been found yet. Therefore, finding a formula or a set of parameters that can efficiently describe and predict DROs and their behavior is desired. The possibilities to do so and the current state of research shall be investigated in this literature review. Therefore, the initial research question is: **How can Distant Retrograde Orbits and their transfers be modeled in order to efficiently predict their behavior and possibly transfers to them?**

This report is structured as follows: Chapter 2 gives an overview of the fundamental astrodynamical laws and concepts that are necessary to understand DROs, Hamiltonian mechanics and stability of closed orbits. Chapter 3 then treats DROs in particular with the knowledge of Chapter 2. It is discussed how to come up with initial conditions for DROs and their stability (regions). Chapter 4 presents the two existing techniques of modeling DROs together with their respective advantages and disadvantages. The transfer to DROs is discussed in Chapter 5, taking into account different starting points. For the further analysis of the problem a numerical propagation will be needed, whose details are explained in Chapter 6. When it comes to trajectory design, an optimizer is needed in order to find the optimal solution. Several options how to accomplish this can be found in Chapter 7. Chapter 8 elaborates on the tools that will be used such as Tudat and MATLAB. Finally, in Chapter 9 the most important conclusions are drawn and the research questions are being updated based on the knowledge that was gained during this literature study. It also contains a preliminary planing of the thesis project.

2

Astrodynamics

Astrodynamics or *Orbital Mechanics* is the science that deals with the movement of celestial bodies with respect to each other. This includes natural bodies like the Sun, the planets, their moons and human-made objects like rockets and satellites. The underlying fundamental physical laws are explained in the next two sections, followed by four sections that deal with more specific problems that are important to understand before dealing with DROs in the next chapter.

2.1. Fundamental Physical Laws

Sir Isaac Newton described in [43] the fundamental laws of motion. The second of which puts the mass m of a body, its total acceleration vector $\mathbf{a}$ and the sum of all forces $\mathbf{F}$ acting on the body in relation:

$$\mathbf{F} = m\mathbf{a} \tag{2.1}$$

This requires the mass m to be constant which is a good assumption for celestial bodies. It is not a good assumption for rockets during the propellant-ejecting propulsion phase. Nevertheless, Newtonian mechanics can still be applied in this case using the solidification principle.

To evaluate the acceleration $\mathbf{a}$ of a body, the sum of the forces $\mathbf{F}$ acting on it has to be evaluated. The most prominent contribution to this is the gravitational force, investigated by Newton. It implies that all objects with mass attract each other, with the magnitude F of the force $\mathbf{F}$ acting between two bodies with masses m_1 and m_2 being:

$$F = G\frac{m_1 m_2}{r^2} \tag{2.2}$$

The force is directed into the direction of the other body, respectively. r is the distance between the two bodies and $G = 6.67428 \cdot 10^{-11}\,\mathrm{m^3/kg\,s^2}$ ([56], Table B.1) is the universal gravitational constant. It is important to note that the gravitational forces do not only occur between two point masses. Every mass in a system attracts every other mass. Usually, the heaviest of them is treated as the *main body* which makes the gravitational attractions exerted by the other bodies *third body perturbations*. Furthermore, no body actually behaves as a point mass, this can and can not be a good approximation depending on the problem. The uneven mass distribution inside a body can be taken into account with spherical harmonics gravity which is briefly explained in Section 2.6.

Another force that might play a role for the deeper analysis of DROs is the solar radiation pressure. This is based on the exchange of momentum that a spacecraft or a celestial body and the solar radiation have. It is typically modeled as being proportional to the inverse squared of the distance to the Sun. The proportionality constant depends on the well known Solar radiation on the one hand and on the surface (area, shape, material, orientation, etc.) of the body on the other hand.

The order of magnitude of the mentioned forces is investigated in Section 2.6. Other forces that can typically play a role in astrodynamics as for example atmospheric drag are not expected to be of importance for DROs.

2.2. Two-Body Problem

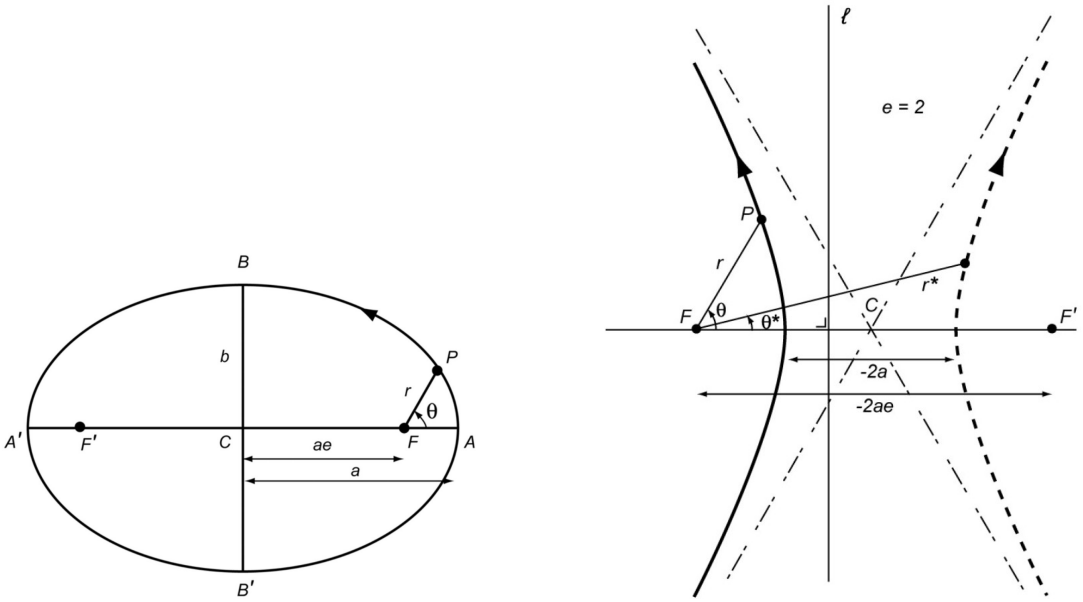

Figure 2.1: Depiction of the Kepler elements semi-major axis a, eccentricity e, and true anomaly θ for an elliptic orbit (left) and a hyperbolic orbit (right). [56]

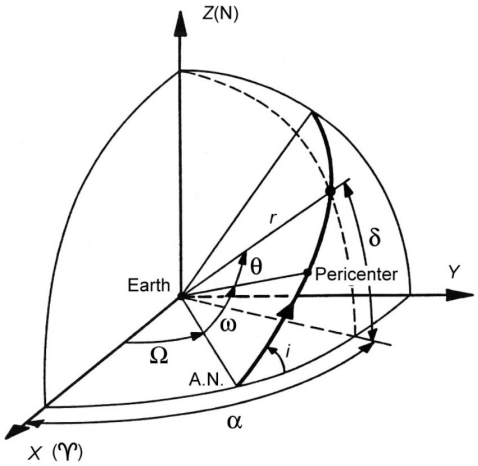

Figure 2.2: Depiction of the Kepler elements RAAN Ω, arguments of periapsis ω, true anomaly θ, and inclination i. [56]

Considering the gravitational forces from Equation (2.2) only, and disregarding all other forces, already yields a problem that is generally not analytically solvable – the n-body problem. However, if the number of involved bodies is restricted to two, the system does have an analytical solution. The family of solutions is called Kepler orbits. Their full descriptions and derivations can be found in [56]. All solutions have in common that the two bodies perform a movement about their barycenter. If the mass of one of the bodies is by far larger than the one of the other body, a commonly made simplifying assumption is that only the lighter body performs a movement about the heavier body's center of gravity. Any constellation can be characterized by six parameters (Kepler elements) of which the eccentricity e indicates the shape of the movement: $e = 0$ implies circular orbits, $0 < e < 1$ implies elliptic orbits, $e = 1$ implies parabolic orbits, and $e > 1$ implies hyperbolic orbits. The size of the respective orbit is manifested in the semi-major axis a with different definitions for the different shapes. Those can be seen in Figure 2.1. Another three elements – namely the inclination i, the right ascension of the ascending node (RAAN) Ω, and the argument of periapsis ω – represent the orientation of the orbit in space. Their meaning can be identified in Figure 2.2. Finally, the anomaly (true anomaly θ, mean

anomaly M, or eccentric anomaly E) indicates at what point in their orbit the two objects (or only the lighter object, if the heavier object is assumed not to move) are.

With the true anomaly θ being the angle between periapsis (the closest approach of the two bodies) and their current position, the distance r between the two bodies can be obtained by

$$r = \frac{p}{1 + e\cos\theta} \tag{2.3}$$

with p being the semi-latus rectum, which corresponds to the distance r in the case $\theta = \pm\pi/2$. Unlike the semi-major axis a – which causes problems for parabolic orbits –, it is defined properly for all shapes of orbits. For elliptic (including circular) and hyperbolic orbits, p can be calculated by

$$p = a\left(1 - e^2\right) \tag{2.4}$$

while for parabolic orbits – since a is not properly defined in the first place – Equation (2.3) is a better representation of the orbit than the Kepler elements. However, parabolic orbits are rare and one might even argue they are impossible to achieve since the eccentricity has to be precisely 1 – and this does not even take perturbations into account.

2.3. Circular Restricted Three-Body Problem

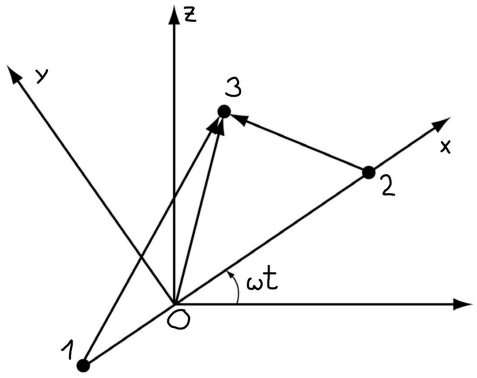

Figure 2.3: Depiction of the coordinate axes in the Circular Restricted Three-Body Problem. The origin O is at the barycenter of the primary (1) and the secondary (2), with all three of them lying on the x-axis. The coordinate system – in which the position of the third body (3) is expressed – is rotating about the z-axis with angular velocity ω. [56]

When three bodies are involved, no analytical solution can be found. The Circular Restricted Three-Body Problem (CR3BP) (see [56], chapter 3) aims to simplify this situation as much as possible in order to make at least some general statements about the orbits of those three bodies. The underlying assumptions for this problem are:

- The mass of the third body (for example a spacecraft) is negligibly small, thus the other two bodies (called *primaries* in this text) are not influenced by the third body.
- The primaries perform a circular movement about their common barycenter with the eccentricity e being 0.

The author refers to the primaries as *primary* and *secondary* with primary being the heavier body. The coordinate system can be seen in Figure 2.3 and is chosen as such: the origin is located in the barycenter of the primaries. The z-axis is pointing in the direction of the angular momentum vector of the primaries, thus perpendicular to their orbital plane. The x-axis is pointing from the primary to the secondary and the y-axis is pointing in the direction of velocity of the secondary. Thus, the used coordinate system is orthogonal and follows the right-hand rule. Furthermore, it is rotating around the z-axis with the same angular velocity ω as the system of primaries. It is apparent that the positions of the primaries in this coordinate system are fixed and depend on their distance and their mass fraction. To get rid of the former, all quantities can be nondimensionalized with the unit of distance being the

distance between the two primaries. The unit of time will be $1/\omega$ and the unit of mass will be the sum of the masses m_1 and m_2 of the two primaries. Now, the position of the two primaries only depends on their mass fraction μ, defined as:

$$\mu = \frac{m_2}{m_1 + m_2} \tag{2.5}$$

The coordinates $\mathbf{c_1}$ and $\mathbf{c_2}$ of the primary and the secondary are then constant:

$$\mathbf{c_1} = \begin{bmatrix} -\mu \\ 0 \\ 0 \end{bmatrix} \quad \text{and} \quad \mathbf{c_2} = \begin{bmatrix} 1-\mu \\ 0 \\ 0 \end{bmatrix} \tag{2.6}$$

2.3.1. Equations of Motion and Potential

The equations of motion for the third body are (from [56], Equation (3.46)):

$$\ddot{x} = \underbrace{x}_{\text{centrifugal}} \underbrace{- \frac{1-\mu}{r_1^3}(\mu + x) + \frac{\mu}{r_2^3}(1-\mu-x)}_{\text{gravitational}} \underbrace{+ 2\dot{y}}_{\text{coriolis}} \tag{2.7}$$

$$\ddot{y} = \underbrace{y}_{\text{centrifugal}} \underbrace{- \frac{1-\mu}{r_1^3} y - \frac{\mu}{r_2^3} y}_{\text{gravitational}} \underbrace{- 2\dot{x}}_{\text{coriolis}} \tag{2.8}$$

$$\ddot{z} = \underbrace{- \frac{1-\mu}{r_1^3} z - \frac{\mu}{r_2^3} z}_{\text{gravitational}} \tag{2.9}$$

with r_1 and r_2 being the distances between the third body and the primaries:

$$r_1 = \sqrt{(\mu + x)^2 + y^2 + z^2} \quad \text{and} \quad r_2 = \sqrt{(1-\mu-x)^2 + y^2 + z^2} \tag{2.10}$$

The gravitational and the centrifugal component of the force are conservative forces, meaning the energy needed to move a particle in this force field only depends on start and end of the movement, but not on the path taken. Therefore, each point in space (in the rotating coordinate frame) can be connected to a potential level, and the potential difference between two points yields the energy needed. The potential U is then:

$$U = \underbrace{\frac{1}{2}(x^2 + y^2)}_{\text{centrifugal}} \underbrace{+ \frac{1-\mu}{r_1} + \frac{\mu}{r_2}}_{\text{gravitational}} \tag{2.11}$$

With this, Equations (2.7) to (2.9) can be rewritten to be:

$$\begin{bmatrix} \ddot{x} - 2\dot{y} \\ \ddot{y} + 2\dot{x} \\ \ddot{z} \end{bmatrix} = \nabla U = \begin{bmatrix} \partial U/\partial x \\ \partial U/\partial y \\ \partial U/\partial z \end{bmatrix} \tag{2.12}$$

2.3.2. Jacobi Constant

While the two-body problem allows for the evaluation of five constants and one time-dependent variable (anomaly), the CR3BP has only one constant, the so-called Jacobi constant C (from [56], Equation (3.54)):

$$C = 2U - \left(\dot{x}^2 + \dot{y}^2 + \dot{z}^2\right) = x^2 + y^2 + \frac{2(1-\mu)}{r_1} + \frac{2\mu}{r_2} - \left(\dot{x}^2 + \dot{y}^2 + \dot{z}^2\right) \tag{2.13}$$

Thus, no matter what value the Jacobi constant takes, with no perturbations in the CR3BP, it will stay at this value forever. This will be useful for the analysis of some DROs.

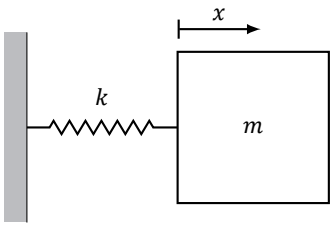

Figure 2.4: Mass spring system with mass m and spring constant k.

2.3.3. Lagrangian and Hamiltonian Dynamics

A different way of describing the motion of objects in force fields can be found in the Lagrangian and Hamiltonian dynamics. Instead of connecting the acceleration to the force like in Newton's second law (Equation (2.1)), Hamiltonian dynamics copes without the concept of forces. Instead, any configuration of bodies is described with kinetic energy T and potential energy V. The Lagrangian $\mathcal{L}$ – named after the first person to investigate it, Joseph-Louis Lagrange ([28, 29]) – is the difference between kinetic and potential energy:

$$\mathcal{L} = T - V \tag{2.14}$$

With the state space (typically) consisting of position components (in the diction of Hamiltonian mechanics *generalized coordinates*) q_i and velocity components $\dot{q}_i$, the path between two states at two times t_1 and t_2 is the one that minimizes the integral

$$\int_{t_1}^{t_2} \mathcal{L} \, \mathrm{d}x \tag{2.15}$$

It can be shown that this corresponds to the following condition (from [52], chapter 6):

$$\frac{\mathrm{d}}{\mathrm{d}t}\frac{\partial \mathcal{L}}{\partial \dot{q}_i} - \frac{\partial \mathcal{L}}{\partial q_i} = 0 \tag{2.16}$$

Hamiltonian mechanics, formulates by William Rowan Hamilton, builds on Lagrangian mechanics. The Hamiltonian $\mathcal{H}$ is defined as:

$$\mathcal{H}\left(q, p, t\right) = \dot{q}_i p_i - \mathcal{L}\left(q, \dot{q}, t\right) \tag{2.17}$$

with p_i being the *generalized momenta*, defined as:

$$p_i = \frac{\partial \mathcal{L}\left(q_j, \dot{q}_j, t\right)}{\partial \dot{q}_i} \tag{2.18}$$

The names *generalized coordinates* and *generalized momenta* for q_i and p_i can be understood when regarding a very simple system. As an example, a mass m that is connected to a wall through a spring with spring constant k is taken. This can be seen in Figure 2.4. An equation for the displacement x of the mass can easily be obtained with Newton's second law:

$$m\ddot{x} = -kx \tag{2.19}$$

Taking x as the only generalized coordinate of this problem, the Lagrangian $\mathcal{L}$ will be:

$$\mathcal{L} = T - V = \frac{1}{2}m\dot{x}^2 - \frac{1}{2}kx^2 \tag{2.20}$$

Equation (2.16) gives then

$$\frac{\mathrm{d}}{\mathrm{d}t}\frac{\partial \mathcal{L}}{\partial \dot{x}} - \frac{\partial \mathcal{L}}{\partial x} = \frac{\mathrm{d}}{\mathrm{d}t}\left(m\dot{x}\right) - \left(-kx\right) = m\ddot{x} + kx = 0, \tag{2.21}$$

which is obviously equivalent to Equation (2.19). Now, evaluating Equation (2.18) for this problem, with the only generalized momentum being p, yields:

$$p = \frac{\partial \mathcal{L}\left(x, \dot{x}, t\right)}{\partial \dot{x}} = \frac{\partial}{\partial \dot{x}}\left(\frac{1}{2}m\dot{x}^2 - \frac{1}{2}kx^2\right) = m\dot{x} \tag{2.22}$$

Thus, in this simple example, the generalized momentum corresponds with the classical momentum of a mass. This is not necessarily the case for more complex systems, but it shows where the name *generalized momenta* comes from.

In general, the rate of change of the Hamiltonian $\mathcal{H}$ can be computed to be ([52], Chapter 6)

$$\frac{\mathrm{d}\mathcal{H}}{\mathrm{d}t} = -\frac{\partial \mathcal{L}}{\partial t} \tag{2.23}$$

which *in particular* for time-independent systems means that $\mathcal{H}$ is constant. For example, in the mass spring system, $\mathcal{H}$ happens to be the total energy of the system:

$$\mathcal{H}\left(x,p,t\right) = \dot{x}p - \mathcal{L}\left(x,\dot{x},t\right) = m\dot{x}^2 - \left(\frac{1}{2}m\dot{x}^2 - \frac{1}{2}kx^2\right) = \frac{1}{2}m\dot{x}^2 + \frac{1}{2}kx^2 = T + V \tag{2.24}$$

The rate of change of the Hamiltonian $\mathcal{H}$ in this specific case can be determined to be zero by either applying Equation (2.23) to Equation (2.20) or by applying the law of conservation of energy to Equation (2.24).

A Hamiltonian system is described by the following equations (from [19]):

$$\frac{\mathrm{d}p_i}{\mathrm{d}t} = -\frac{\partial \mathcal{H}}{\partial q_i} \qquad \text{and} \qquad \frac{\mathrm{d}q_i}{\mathrm{d}t} = \frac{\partial \mathcal{H}}{\partial p_i} \tag{2.25}$$

The Hamiltonian $\mathcal{H}$ that belongs to the CR3BP is ([8, 33, 52]):

$$\mathcal{H} = \frac{1}{2}\left(X^2 + Y^2 + Z^2\right) - xY + yX + \Phi\left(x,y,z\right) \tag{2.26}$$

Here, the xyz coordinate system is defined as in the beginning of this chapter and rotates about the z-axis. The potential Φ is defined in Equation (2.29). x, y and z represent the position of the third body in the rotating coordinate system. X, Y and Z are their generalized momenta. They represent the velocity of the third body in an inertial reference frame but expressed in the rotating coordinate system ([52], p. 349). Thus, with the nondimensionalization as described before (which implies that $\omega = 1$), the relation between $\dot{x}$, $\dot{y}$, $\dot{z}$ and X, Y, Z is:

$$\begin{bmatrix} X \\ Y \\ Z \end{bmatrix} = \begin{bmatrix} \dot{x} \\ \dot{y} \\ \dot{z} \end{bmatrix} + \begin{bmatrix} 0 \\ 0 \\ 1 \end{bmatrix} \times \begin{bmatrix} x \\ y \\ z \end{bmatrix} = \begin{bmatrix} \dot{x} - y \\ \dot{y} + x \\ \dot{z} \end{bmatrix} \tag{2.27}$$

It is not surprising that $\dot{z}$ and Z are equivalent, since the z-axis is not moving. Also, the (nondimensional) velocities $\dot{x}$, $\dot{y}$ and $\dot{z}$ are *naturally* related to the (nondimensional) generalized momenta X, Y and Z, since the nondimensionalization of the momenta takes away the mass and thus leaves only the velocity. The reverse relation is:

$$\begin{bmatrix} \dot{x} \\ \dot{y} \\ \dot{z} \end{bmatrix} = \begin{bmatrix} X + y \\ Y - x \\ Z \end{bmatrix} \tag{2.28}$$

The potential $\Phi(x,y,z)$ in Equation (2.26) takes only gravitational potential into account. This is in contrast to the potential U as defined in Equation (2.11). The term $-xY + yX$ includes the centrifugal force. Notice also the different sign between U and Φ. This makes the potential

$$\Phi\left(x,y,z\right) = -\frac{1-\mu}{r_1} - \frac{\mu}{r_2} \tag{2.29}$$

and its partial derivatives:

$$\frac{\partial \Phi}{\partial x} = \frac{\left(1-\mu\right)\left(x+\mu\right)}{r_1^3} + \frac{\mu\left(x-1+\mu\right)}{r_2^3}, \qquad \frac{\partial \Phi}{\partial y} = \frac{\left(1-\mu\right)y}{r_1^3} + \frac{\mu y}{r_2^3}, \qquad \text{and} \qquad \frac{\partial \Phi}{\partial z} = \frac{\left(1-\mu\right)z}{r_1^3} + \frac{\mu z}{r_2^3} \tag{2.30}$$

This being said, inserting the Hamiltonian $\mathcal{H}$ from Equation (2.26) into the three equations on the right-hand side of Equation (2.25) yields:

$$\dot{x} = \frac{\mathrm{d}x}{\mathrm{d}t} = \frac{\partial \mathcal{H}}{\partial X} = X + y, \qquad \dot{y} = \frac{\mathrm{d}y}{\mathrm{d}t} = \frac{\partial \mathcal{H}}{\partial Y} = Y - x, \qquad \text{and} \qquad \dot{z} = \frac{\mathrm{d}z}{\mathrm{d}t} = \frac{\partial \mathcal{H}}{\partial Z} = Z \tag{2.31}$$

Those relations were already known by the considerations on velocities in the fixed and the rotating coordinate system that were shown in Equation (2.27). However, using the three equations on the left-hand side of Equation (2.25) yields the new equations:

$$\dot{X} = \frac{\mathrm{d}X}{\mathrm{d}t} = -\frac{\partial \mathcal{H}}{\partial x} = Y - \frac{(1-\mu)\,(x+\mu)}{r_1^3} - \frac{\mu\,(x-1+\mu)}{r_2^3} \tag{2.32}$$

$$\dot{Y} = \frac{\mathrm{d}Y}{\mathrm{d}t} = -\frac{\partial \mathcal{H}}{\partial y} = -X - \frac{(1-\mu)\,y}{r_1^3} - \frac{\mu y}{r_2^3} \tag{2.33}$$

$$\dot{Z} = \frac{\mathrm{d}Z}{\mathrm{d}t} = -\frac{\partial \mathcal{H}}{\partial z} = -\frac{(1-\mu)\,z}{r_1^3} - \frac{\mu z}{r_2^3} \tag{2.34}$$

Deriving Equation (2.31) with respect to time and inserting Equations (2.32) to (2.34) yields:

$$\ddot{x} = \dot{X} + \dot{y} = Y - \frac{(1-\mu)\,(x+\mu)}{r_1^3} - \frac{\mu\,(x-1+\mu)}{r_2^3} + \dot{y} = -\frac{(1-\mu)\,(x+\mu)}{r_1^3} - \frac{\mu\,(x-1+\mu)}{r_2^3} + 2\dot{y} + x \tag{2.35}$$

$$\ddot{y} = \dot{Y} + \dot{x} = -X - \frac{(1-\mu)\,y}{r_1^3} - \frac{\mu y}{r_2^3} + \dot{x} = -\frac{(1-\mu)\,y}{r_1^3} - \frac{\mu y}{r_2^3} - 2\dot{x} + y \tag{2.36}$$

$$\ddot{z} = \dot{Z} = -\frac{(1-\mu)\,z}{r_1^3} - \frac{\mu z}{r_2^3} \tag{2.37}$$

These equations are the same as Equations (2.7) to (2.9), which confirms the Hamiltonian mechanics for the CR3BP. Hamiltonian mechanics is not better or worse than Newtonian mechanics. These are just two different ways of mathematically describing the same physical effects and relations. While Newtonian mechanics is usually easier to be understood, Hamiltonian mechanics can open the door to a new realm of options for analyzing a problem. This strongly depends on the problem itself and can not be generalized. For DROs in particular, [32, 34] state that the accuracy with which DROs can be analyzed improves when taking the Hamiltonian instead of Newtonian perspective.

2.4. Planar Hill Problem

The problem of Hill ([23]) as described in [22] is a more specific problem than the CR3BP. It assumes that also the mass of the secondary is *small*. Therefore, gravitational attraction between the secondary and the third body is lower in order than the attraction exerted by the primary *unless* the secondary and the third body are close to each other, which is exactly what the problem of Hill is about. The problem of Hill is less specific than the CR3BP in one regard: the secondary does not have to move on a circular path around the primary, its orbit just needs to be *close* to being circular (as well as the one of the third body). In fact, according to [22], p. 71, the secondary and the third body are supposed to be “in the vicinity of point (1,0)” (of the previously defined rotating coordinate system). The *Planar* Hill Problem, which is discussed in the following is restricted to take place in the orbital plane of the primaries. Therefore, $z = 0$.

2.4.1. Equations of Motion

Since now both the secondary and the third body have a *small* mass, their masses have the same order of magnitude and thus their mass ratio gets important. This new parameter will be called ν:

$$\nu = \frac{m_3}{m_2 + m_3} \tag{2.38}$$

Also, the mass ratio μ has to take m_3 into account now:

$$\mu = \frac{m_2 + m_3}{m_1 + m_2 + m_3} \tag{2.39}$$

To account for the new specifics of the problem, another change of the coordinate system is performed. It is centered at the point (1,0) (in the rotating xy-coordinate system). It should be noticed, that this is a point at which a small point mass could stay – meaning that the point (1,0) in the rotating coordinate system has the exact rotational speed that is needed to orbit the primary. Since the problem is now of local nature, the distance between the primary and the secondary is not a good scale for distance anymore. Instead, the radius, within which the secondary and the third body are the main gravitational force for each other (instead of the primary) is taken. This radius is know as radius of Hill ([23]). In the rotating xy-coordinate frame, it happens to be $\mu^{1/3}$ ([22]), which is going to be the new unit in the new coordinate system. Therefore, the new coordinate system $\xi\eta$ is defined with:

$$x = 1 + \mu^{\frac{1}{3}}\xi \qquad \text{and} \qquad y = \mu^{\frac{1}{3}}\eta \tag{2.40}$$

In this new coordinate system, the equation of motion for the secondary (index 2) are (from [22]):

$$\ddot{\xi}_2 = 2\dot{\eta}_2 + 3\xi_2 + \frac{\nu\,(\xi_3 - \xi_2)}{\rho^3} + \mathcal{O}\left(\mu^{\frac{1}{3}}\right) \qquad \text{and} \qquad \ddot{\eta}_2 = -2\dot{\xi}_2 + \frac{\nu\,(\eta_3 - \eta_2)}{\rho^3} + \mathcal{O}\left(\mu^{\frac{1}{3}}\right) \tag{2.41}$$

And equivalent for the third body:

$$\ddot{\xi}_3 = 2\dot{\eta}_3 + 3\xi_3 + \frac{(1-\nu)\,(\xi_2 - \xi_3)}{\rho^3} + \mathcal{O}\left(\mu^{\frac{1}{3}}\right) \qquad \text{and} \qquad \ddot{\eta}_3 = -2\dot{\xi}_3 + \frac{(1-\nu)\,(\eta_2 - \eta_3)}{\rho^3} + \mathcal{O}\left(\mu^{\frac{1}{3}}\right) \tag{2.42}$$

with ρ being the distance between the secondary and the third body in the new coordinates. Defining new coordinates with ξ^* and η^* being the position of the center of gravity of the secondary and the third body and ξ and η being their relative position yields simpler equations of motion ([22], Equation (19)):

$$\xi^* = (1-\nu)\,\xi_2 + \nu\xi_3 \qquad \text{and} \qquad \eta^* = (1-\nu)\,\eta_2 + \nu\eta_3 \qquad \text{and} \qquad \xi = \xi_3 - \xi_2 \qquad \text{and} \qquad \eta = \eta_3 - \eta_2 \tag{2.43}$$

With this, the equations of motion simplify to ([22], Equations (20) and (21), which can easily be verified by combining Equations (2.41) to (2.43)):

$$\ddot{\xi}^* = 2\dot{\eta}^* + 3\xi^* + \mathcal{O}\left(\mu^{\frac{1}{3}}\right) \qquad \text{and} \qquad \ddot{\eta}^* = -2\dot{\xi}^* + \mathcal{O}\left(\mu^{\frac{1}{3}}\right) \tag{2.44}$$

$$\ddot{\xi} = 2\dot{\eta} + 3\xi - \frac{\xi}{\rho^3} + \mathcal{O}\left(\mu^{\frac{1}{3}}\right) \qquad \text{and} \qquad \ddot{\eta} = -2\dot{\xi} - \frac{\eta}{\rho^3} + \mathcal{O}\left(\mu^{\frac{1}{3}}\right) \tag{2.45}$$

Assuming that the mass of the primary is much bigger than the masses of the other two bodies means that μ is small and thus $\mathcal{O}(\mu^{1/3})$ can be neglected. Then, the motion of the barycenter of the secondary and the third body – ξ^* and η^* – can be solved analytically. More interesting is the relative motion ξ and η of these two bodies. This is known as the Hill equations:

$$\ddot{\xi} = 2\dot{\eta} + 3\xi - \frac{\xi}{\rho^3} \qquad \text{and} \qquad \ddot{\eta} = -2\dot{\xi} - \frac{\eta}{\rho^3} \tag{2.46}$$

One may notice, that if the last term – which represents the gravitational attraction between the secondary and the third body – is neglected, the equations are equivalent to the Clohessy-Wiltshire equations for the relative motion of two satellites in close-to-circular orbits. According to [56], they were rediscovered by Clohessy and Wiltshire in 1960 ([12]) after being found first by Hill in [23].

2.4.2. Jacobi Integral

Like the CR3BP, also the Hill problem has a constant that does not change with time. According to [22], it is Γ being:

$$\Gamma = 3\xi^2 + \frac{2}{\rho} - \dot{\xi}^2 - \dot{\eta}^2 \tag{2.47}$$

With

$$\frac{\mathrm{d}\frac{1}{\rho}}{\mathrm{d}t} = \frac{\mathrm{d}\left(\xi^2 + \eta^2\right)^{-\frac{1}{2}}}{\mathrm{d}t} = -\frac{1}{2}\left(\xi^2 + \eta^2\right)^{-\frac{3}{2}}\left(2\xi\dot{\xi} + 2\eta\dot{\eta}\right) = \frac{-\xi\dot{\xi} - \eta\dot{\eta}}{\rho^3} \tag{2.48}$$

and Equation (2.46) it can easily be shown that indeed Γ does not change with time:

$$\frac{\mathrm{d}\Gamma}{\mathrm{d}t} = 6\xi\dot{\xi} + 2\frac{-\xi\dot{\xi} - \eta\dot{\eta}}{\rho^3} - 2\dot{\xi}\ddot{\xi} - 2\dot{\eta}\ddot{\eta} = 6\xi\dot{\xi} + 2\frac{-\xi\dot{\xi} - \eta\dot{\eta}}{\rho^3} - 2\dot{\xi}\left(2\dot{\eta} + 3\xi - \frac{\xi}{\rho^3}\right) - 2\dot{\eta}\left(-2\dot{\xi} - \frac{\eta}{\rho^3}\right) =$$
$$= \left(6\xi\dot{\xi} - 4\dot{\xi}\dot{\eta} - 6\dot{\xi}\xi + 4\dot{\eta}\dot{\xi}\right) + \frac{1}{\rho^3}\left(-2\xi\dot{\xi} - 2\eta\dot{\eta} + 2\dot{\xi}\xi + 2\dot{\eta}\eta\right) = 0 \tag{2.49}$$

2.4.3. Hamiltonian Dynamics

Like in the CR3BP, the planar Hill problem can be described using Hamiltonian mechanics as well. This is commonly expressed with the coordinates x and y and their conjugate momenta X and Y. The coordinates x and y correspond to the previously defined coordinates ξ and η. Then, according to [8, 52], the Hamiltonian $\mathcal{H}$ is:

$$\mathcal{H} = \frac{1}{2}(X + y)^2 + \frac{1}{2}(Y - x)^2 - \frac{3}{2}x^2 + \Phi(x, y) \tag{2.50}$$

with

$$\Phi(x, y) = -\frac{1}{r} \quad \text{and} \quad r = \sqrt{x^2 + y^2} \tag{2.51}$$

This can easily be confirmed by solving the following partial differentials:

$$\dot{x} = \frac{\partial\mathcal{H}}{\partial X} = X + y, \quad \dot{y} = \frac{\partial\mathcal{H}}{\partial Y} = Y - x, \quad \dot{X} = -\frac{\partial\mathcal{H}}{\partial x} = Y + 2x - \frac{x}{r^3}, \quad \dot{Y} = -\frac{\partial\mathcal{H}}{\partial y} = -X - y - \frac{y}{r^3} \tag{2.52}$$

With $X = \dot{x} - y$ and $Y = \dot{y} + x$ it follows:

$$\ddot{x} = \dot{X} + \dot{y} = \ldots = 2\dot{y} + 3x - \frac{x}{r^3} \quad \text{and} \quad \ddot{y} = \dot{Y} - \dot{x} = \ldots = -2\dot{x} - \frac{y}{r^3} \tag{2.53}$$

which is in line with the findings from Equation (2.46).

2.5. Stability of Closed Orbits

The stability of a closed orbit (as for example a DRO) can be analyzed numerically. Therefore it is necessary to propagate the state $\mathbf{X}$ for the duration of one revolution. As a state $\mathbf{X}$, a vector containing three (or two) position components and three (or two) velocity components is taken. This can be in any properly defined coordinate system, for example:

$$\mathbf{X} = \begin{bmatrix} X_1 & X_2 & X_3 & X_4 & X_5 & X_6 \end{bmatrix}^\mathsf{T} = \begin{bmatrix} x & y & z & \dot{x} & \dot{y} & \dot{z} \end{bmatrix}^\mathsf{T} \tag{2.54}$$

With the accelerations $\ddot{x}(\mathbf{X})$, $\ddot{y}(\mathbf{X})$ and $\ddot{z}(\mathbf{X})$ obtained from one of the equations of motions mentioned previously, the state can be propagated using the following system of first-order differential equations:

$$\dot{\mathbf{X}} = \begin{bmatrix} \dot{X}_1 \\ \dot{X}_2 \\ \dot{X}_3 \\ \dot{X}_4 \\ \dot{X}_5 \\ \dot{X}_6 \end{bmatrix} = \begin{bmatrix} \dot{x} \\ \dot{y} \\ \dot{z} \\ \ddot{x} \\ \ddot{y} \\ \ddot{z} \end{bmatrix} = \begin{bmatrix} X_4 \\ X_5 \\ X_6 \\ \ddot{x}(\mathbf{X}) \\ \ddot{y}(\mathbf{X}) \\ \ddot{z}(\mathbf{X}) \end{bmatrix} \tag{2.55}$$

The state transition matrix $\mathbf{\Phi}(t, t_0)$ at any time t gives the change of state at time t that would occur for a change of state at time t_0:

$$\mathbf{\Phi}(t, t_0) = \frac{\partial\mathbf{X}(t)}{\partial\mathbf{X}(t_0)} \quad \text{or} \quad \Phi_{i,j}(t, t_0) = \frac{\partial X_i(t)}{\partial X_j(t_0)} \quad \forall i, j \in (1, 6) \tag{2.56}$$

The state transition matrix can be propagated using (taken from [45], Chapter 2):

$$\dot{\mathbf{\Phi}}(t, t_0) = \frac{\partial\dot{\mathbf{X}}(t)}{\partial\mathbf{X}(t)}\mathbf{\Phi}(t, t_0) \tag{2.57}$$

The starting point of this propagation is given by the definition of the state transition matrix $\mathbf{\Phi}(t_0, t_0)$ to be:

$$\mathbf{\Phi}(t_0, t_0) = \mathbf{I}_{6\times 6} \tag{2.58}$$

The monodromy matrix $\mathbf{M}$ (see [45], Section 2.6.8) is a special case of the state transition matrix. In fact, it is the state transition matrix $\mathbf{\Phi}(T, t_0)$ after the time T of one full (periodic) revolution; therefore at a time at which the state is exactly the same as in the beginning. Then the eigenvalues of this matrix tell if a perturbation gets larger with time (for the real part of an eigenvalue being greater than 1 or smaller than -1), stays the same in magnitude (for the real part being equal to 1 or -1) or decreases with time (for the real part being between -1 and 1), if its sign changes each orbit (for the real part being smaller than 0) or not (for the real part being greater than 0), and if the state vector oscillates with each orbit (for eigenvalues having an imaginary part). The six eigenvalues λ_1 to λ_6 of the monodromy matrix fulfill the following equations ([45], Equation (2.45)):

$$\lambda_1 = \frac{1}{\lambda_2} \quad \text{and} \quad \lambda_3 = \frac{1}{\lambda_4} \quad \text{and} \quad \lambda_5 = \lambda_6 = 1 \tag{2.59}$$

For every eigenvalue that is not 1, a stable (<1) or unstable (>1) manifold can be computed. A manifold is the entirety of the trajectories that enter or leave a closed orbit. They can be computed by altering the state by a (very small) increment into the direction of the eigenvectors that belong to the respective eigenvalue. Since this can be done on every point of the orbit, a collection of trajectories is obtained. For stable manifolds, the propagation has to be performed backwards in time; unstable manifolds are obtained by forward integration. Manifolds are addressed further in Section 3.3.

2.6. Order of Magnitude of Occurring Accelerations for Earth-Moon Distant Retrograde Orbit

Table 2.1: The (maximal possible) acceleration related to the two main body attractions (Earth and Moon) in an Earth-Moon DRO and the accelerations related to perturbations as attractions from other Solar System bodies, Earth's spherical harmonics gravity field and solar radiation pressure. Where ever it makes a difference, it is distinguished between two different DRO sizes and two different bodies (an example spacecraft and an example asteroid) that perform the DRO. The main body attraction parameters can be found in [56], Appendix B and the coefficients for Earth's spherical harmonics gravity field can be found in [53]. Abbreviations: point mass gravity (p.m.g), solar radiation pressure (s.r.p.), spacecraft (S/C). Spherical harmonics gravity is referred to as the $J_{l,m}$ effect.

source	specification	distance to source d	(max) acceleration a [m/s^2]
Moon p.m.g.	big DRO	$192\,\text{Mm} < d < 384\,\text{Mm}$	$3.3 \cdot 10^{-5} < a < 1.3 \cdot 10^{-4}$
	small DRO	$10\,\text{Mm} < d < 20\,\text{Mm}$	$0.012 < a < 0.049$
Earth p.m.g.	big DRO	$192\,\text{Mm} < d < 576\,\text{Mm}$	$0.0012 < a < 0.011$
	small DRO	$374\,\text{Mm} < d < 394\,\text{Mm}$	$0.0026 < a < 0.0029$
Sun p.m.g.	–	$d \approx 1\,\text{AU}$	$a \approx 0.0059$
Jupiter p.m.g.	–	$4.2\,\text{AU} < d < 6.2\,\text{AU}$	$1.5 \cdot 10^{-7} < a < 3.2 \cdot 10^{-7}$
s.r.p.	S/C	$d \approx 1\,\text{AU}$	$a \approx 4.5 \cdot 10^{-7}$
	asteroid		$a \approx 7.1 \cdot 10^{-11}$
Venus p.m.g.	–	$0.27\,\text{AU} < d < 1.8\,\text{AU}$	$4.5 \cdot 10^{-9} < a < 2.0 \cdot 10^{-7}$
Earth $J_{2,0}$ effect	big DRO	$192\,\text{Mm} < d < 576\,\text{Mm}$	$4.8 \cdot 10^{-10} < a < 3.9 \cdot 10^{-8}$
	small DRO	$374\,\text{Mm} < d < 394\,\text{Mm}$	$2.2 \cdot 10^{-9} < a < 2.7 \cdot 10^{-9}$
Saturn p.m.g.	–	$8.5\,\text{AU} < d < 10.5\,\text{AU}$	$1.5 \cdot 10^{-8} < a < 2.4 \cdot 10^{-8}$
Mars p.m.g.	–	$0.52\,\text{AU} < d < 2.52\,\text{AU}$	$3.0 \cdot 10^{-10} < a < 7.1 \cdot 10^{-9}$
Mercury p.m.g.	–	$0.61\,\text{AU} < d < 1.4\,\text{AU}$	$5.0 \cdot 10^{-10} < a < 2.7 \cdot 10^{-9}$
Uranus p.m.g.	–	$18\,\text{AU} < d < 20\,\text{AU}$	$6.5 \cdot 10^{-10} < a < 8.0 \cdot 10^{-10}$
Neptune p.m.g.	–	$29\,\text{AU} < d < 31\,\text{AU}$	$3.2 \cdot 10^{-10} < a < 3.6 \cdot 10^{-10}$
Earth $J_{2,2}$ effect	big DRO	$192\,\text{Mm} < d < 576\,\text{Mm}$	$8.0 \cdot 10^{-13} < a < 6.5 \cdot 10^{-11}$
	small DRO	$374\,\text{Mm} < d < 394\,\text{Mm}$	$3.7 \cdot 10^{-12} < a < 4.5 \cdot 10^{-12}$

The thesis will likely deal with Earth-Moon DROs. To have a first idea of the forces that occur in an Earth-Moon DRO, Table 2.1 shows for some selected (main body attractions and) perturbing elements

the norm of the resulting accelerations. Since it is the order of magnitude of those accelerations that is interesting and not so much the exact numbers themselves, many simplifying assumptions have been made in order to come up with this table. Therefore, the *exact numbers* can not be trusted, their approximate values *can* be trusted. The first simplifying assumption regards the shape of the DRO (which has implications on the minimal and maximal distance of the orbit to Earth and Moon). As it is a result of the Hill problem (see Section 4.2) (and therefore not applicable for big distances to the Moon, which is ignored here) the DROs are assumed to have elliptical shape with the semi-major axis being twice the semi-minor axis, Moon being in the center of the ellipse, and the semi-minor axis pointing towards Earth. Two different sized DROs – called "big" and "small" in Table 2.1 – are used which makes a difference only for accelerations that are related to Earth or Moon. The bigger orbit has a semi-minor axis that is half of the Moon's orbital semi-major axis (all planets' orbital parameters have been taken from [56], Appendix B); the smaller orbit has a semi-minor axis of $10\,000$ km (and therefore a semi-major axis of $20\,000$ km). For evaluating the acceleration resulting from solar radiation pressure, assumptions regarding mass, surface area, and kind of surface have to be made. Therefore, two different objects have been analyzed, that might both find themselves in an Earth-Moon DRO one day: a spacecraft (S/C) with a mass of 2000 kg and an effective cross-sectional area of $100\,\mathrm{m}^2$ and an asteroid with a mass of 10^9 kg and an effective cross-sectional area of $7854\,\mathrm{m}^2$, which roughly corresponds to a sphere of radius 50 m and a density of $2\,\mathrm{g/cm}^3$. Depending on the kind of surface, the radiation pressure can be experienced by the body zero times (nothing absorbed or reflected), one time (all radiation absorbed, nothing reflected), two times (all radiation reflected) and anything in between. For Table 2.1 it is assumed that the full solar radiation pressure of $9.08\,\mu$Pa (at Sun-Earth distance, according to [56], Table B.1) is absorbed and not reflected.

Irregularities in the Earth's gravity field are modeled with a spherical harmonics model with the potential U being ([17]):

$$U = \frac{\mu}{r} \sum_{l=0}^{\infty} \sum_{m=0}^{l} \left(\frac{R}{r}\right)^l \bar{P}_{lm}\left(\sin\phi\right)\left(\bar{C}_{lm}\cos m\theta + \bar{S}_{lm}\sin m\theta\right) \tag{2.60}$$

With μ being the product of the Earth's mass and the universal gravitational constant G, R being the Earth's radius, r being the object's distance to the center of Earth, θ and ϕ representing the object's direction as seen from the center of Earth, $\bar{C}_{lm}$ and $\bar{S}_{lm}$ being the Earth's normalized spherical harmonics gravity field coefficients, and $\bar{P}_{lm}$ being normalized associated Legendre polynomials. As a simplification, the acceleration in any direction other than the radial direction is neglected. The acceleration in radial direction is equal to the partial derivative of the potential U with respect to the distance r. Therefore, the contribution to the acceleration that the spherical harmonics gravity term with order l and degree m has is:

$$|a_{lm}| = (l+1)\,\frac{\mu}{r^2}\left(\frac{R}{r}\right)^l \underbrace{\left|\bar{P}_{lm}\left(\sin\phi\right)\right|}_{\leq 1} \underbrace{\left|\bar{C}_{lm}\cos m\theta + \bar{S}_{lm}\sin m\theta\right|}_{\leq \sqrt{\bar{C}_{lm}^2+\bar{S}_{lm}^2}} \leq (l+1)\,\frac{\mu R^l}{r^{l+2}}\sqrt{\bar{C}_{lm}^2+\bar{S}_{lm}^2} \tag{2.61}$$

This has been done knowing that the normalized associated Legendre polynomials are always between -1 and 1. Therefore, an upper bound for the acceleration resulting from the spherical harmonics gravity term of order l and degree m can easily be computed with the inequation in Equation (2.61). Thus, Table 2.1 contains the maximum effect that the selected two spherical harmonics terms can have (the selected two are the biggest ones) – not regarding the direction in which the spacecraft or the asteroid is with respect to Earth. One might notice that the higher the order l, the faster its effect decreases with increasing distance r to Earth. Therefore, higher-order terms do not only have lower normalized gravity coefficients $\bar{C}_{lm}$ and $\bar{S}_{lm}$ in general (see [53]), but their influence is also a smaller fraction of the original influence at the Earth's surface. As a result, all higher orders have for sure a smaller influence. If the coordinate system is chosen correctly, the order-one coefficients are zero. The coefficients for the 2,1 gravity field terms are lower than the ones of the 2,0 and 2,2 gravity terms which makes them the strongest effects for which they are listed in Table 2.1.

In order to understand Table 2.1 correctly, two things are crucial to mention. They put the listed accelerations in the right perspective. Only because one effect has a higher acceleration in the table, it does not mean it is more important to be included in a simulation. The first reason for this is that the accelerations in the table are absolute. For them to be meaningful, the relative acceleration with respect to the primary (in this case the primaries) should be taken into account. Two point masses that exert the same absolute acceleration on the spacecraft can have different relative accelerations. In fact, the smaller mass needs to be closer to the spacecraft in order to exert the same absolute acceleration, and therefore its gravity field's gradient is bigger which implies that the changes in gravitational attraction when switching between spacecraft, Earth and Moon are stronger. Therefore, the relative acceleration that the smaller mass exerts on the spacecraft is larger than the one of the bigger mass. This is counter-intuitive and shows that the incorporated third bodies have to be considered carefully. Analyzing the relative acceleration for each perturbation requires to know which of the primaries should be considered as being the central mass. This might depend on the size of the DRO and will be evaluated at the appropriate time during the thesis.

Secondly, it is not even given that a larger relative acceleration results in a more important perturbation. This is especially not the case when regarding a long time evolution of DROs. Perturbations that are periodic tend to induce bigger changes to regular orbits than perturbations that have a rather erratic behavior. Also, periodic perturbations can happen to exactly cancel themselves out after one orbit. All these arguments show that only looking at Table 2.1 is not enough to evaluate how important certain factors for the numeric propagation are; this will have to be evaluated in a more elaborate way. For example, as mentioned in Section 3.2, the Moon's tides can have a big impact on the long term stability of DROs even though their values are comparably small.

3

General Remarks on Distant Retrograde Orbits

DROs are the subject of the thesis project. They are among the most stable orbits for third bodies in two-body systems and therefore interesting for a broad variety of missions.

3.1. Initial Conditions

In a primary-secondary system, a third body can perform a DRO by orbiting about the secondary in a direction that is opposite to the direction that the secondary is orbiting the primary (thus retrograde). But since the third body is still moving with the secondary about the primary, the secondary and third body are orbiting the primary in prograde direction. There are several methods to obtain numerical initial conditions for a DRO; one of which is presented here.

To come up with the initial conditions for DROs, a differential corrector can be used. This can be found for example in [1, 9, 45, 48]. This works with the CR3BP as well as with the Hill problem, but in order to keep it more general it is shown in the CR3BP here. Because the analytic solutions of DROs are to be found in the xy-plane, the z component will be neglected. Due to symmetry, DROs have to cross the x-axis orthogonally, meaning $\dot{y}$ has to be zero at that specific point. Therefore, an initial guess for the initial conditions of a DRO would be:

$$\mathbf{X}_0 = \begin{bmatrix} x_0 & 0 & 0 & \dot{y}_0 \end{bmatrix}^\mathsf{T} \tag{3.1}$$

The state after propagating for half a revolution (meaning until the y-coordinate is zero for the next time) is denoted with the index $1/2$. At this point, the following state $\mathbf{X}_{1/2}$ and state transition matrix $\mathbf{\Phi}_{1/2}$ will be found (for an explanation of the state transition matrix read Section 2.5):

$$\mathbf{X}_{1/2} = \begin{bmatrix} x_{1/2} \\ 0 \\ \dot{x}_{1/2} \\ \dot{y}_{1/2} \end{bmatrix} \quad \text{and} \quad \mathbf{\Phi}_{1/2} = \frac{\partial \mathbf{X}_{1/2}}{\partial \mathbf{X}_0} = \begin{bmatrix} \Phi_{1,1} & \Phi_{1,2} & \Phi_{1,3} & \Phi_{1,4} \\ \Phi_{2,1} & \Phi_{2,2} & \Phi_{2,3} & \Phi_{2,4} \\ \Phi_{3,1} & \Phi_{3,2} & \Phi_{3,3} & \Phi_{3,4} \\ \Phi_{4,1} & \Phi_{4,2} & \Phi_{4,3} & \Phi_{4,4} \end{bmatrix} \tag{3.2}$$

Since after this half orbit, the velocity in x-direction is supposed to be 0 – again, due to symmetry – the following change $\Delta\mathbf{X}_{1/2}$ in state at the half point should be achieved:

$$\Delta\mathbf{X}_{1/2} = \begin{bmatrix} \sim & 0 & -\dot{x}_{1/2} & \sim \end{bmatrix}^\mathsf{T} \tag{3.3}$$

with the "$\sim$" at the x and $\dot{y}$ position indicating that a change in these components is irrelevant to the problem, while the y position should not change and the $\dot{x}$ position should change with the given value to make it zero. Now with the state transition matrix, the (linearized version of the) change in $\mathbf{X}_{1/2}$ can

be calculated depending on a change $\Delta\mathbf{X}_0$ in initial conditions with:

$$\Delta\mathbf{X}_{1/2} = \begin{bmatrix} \sim \\ 0 \\ -\dot{x}_{1/2} \\ \sim \end{bmatrix} = \mathbf{\Phi}_{1/2}\Delta\mathbf{X}_0 = \mathbf{\Phi}_{1/2}\begin{bmatrix} \Delta x_0 \\ \Delta y_0 \\ \Delta\dot{x}_0 \\ \Delta\dot{y}_0 \end{bmatrix} \tag{3.4}$$

Given that – to fulfill the previously set conditions for this orbit – Δy_0 and $\Delta\dot{x}_0$ have to be zero, and that the position x_0 has been chosen and thus should not be changed, this gives:

$$\begin{bmatrix} \sim \\ 0 \\ -\dot{x}_{1/2} \\ \sim \end{bmatrix} = \mathbf{\Phi}_{1/2}\begin{bmatrix} 0 \\ 0 \\ 0 \\ \Delta\dot{y}_0 \end{bmatrix} = \begin{bmatrix} \Phi_{1,4}\Delta\dot{y}_0 \\ \Phi_{2,4}\Delta\dot{y}_0 \\ \Phi_{3,4}\Delta\dot{y}_0 \\ \Phi_{4,4}\Delta\dot{y}_0 \end{bmatrix} \tag{3.5}$$

This is the equation for the change in state after the exact amount of time has passed that had been needed for the first set of initial conditions to reach the half point of the orbit. With different, new initial conditions this time changes as well and to take this into account, the (linearized) change in time Δt is introduced:

$$\begin{bmatrix} \sim \\ 0 \\ -\dot{x}_{1/2} \\ \sim \end{bmatrix} = \begin{bmatrix} \Phi_{1,4}\Delta\dot{y}_0 \\ \Phi_{2,4}\Delta\dot{y}_0 \\ \Phi_{3,4}\Delta\dot{y}_0 \\ \Phi_{4,4}\Delta\dot{y}_0 \end{bmatrix} + \begin{bmatrix} \dot{x}_{1/2} \\ \dot{y}_{1/2} \\ \ddot{x}_{1/2} \\ \ddot{y}_{1/2} \end{bmatrix}\Delta t \tag{3.6}$$

The accelerations $\ddot{x}_{1/2}$ and $\ddot{y}_{1/2}$ can be read from the equations of motion. Then, the two rows that do not include a "∼" give:

$$\begin{cases} 0 = \Phi_{2,4}\Delta\dot{y}_0 + \dot{y}_{1/2}\Delta t \\ -\dot{x}_{1/2} = \Phi_{3,4}\Delta\dot{y}_0 + \ddot{x}_{1/2}\Delta t \end{cases} \tag{3.7}$$

from which it follows:

$$\Delta t = -\frac{\Delta\dot{y}_0}{\dot{y}_{1/2}}\Phi_{2,4} \tag{3.8}$$

$$-\dot{x}_{1/2} = \Phi_{3,4}\Delta\dot{y}_0 + \ddot{x}_{1/2}\left(-\frac{\Delta\dot{y}_0}{\dot{y}_{1/2}}\Phi_{2,4}\right) = \Delta\dot{y}_0\left(\Phi_{3,4} - \frac{\ddot{x}_{1/2}}{\dot{y}_{1/2}}\Phi_{2,4}\right) \tag{3.9}$$

and therefore:

$$\Delta\dot{y}_0 = \frac{\dot{x}_{1/2}}{\frac{\ddot{x}_{1/2}}{\dot{y}_{1/2}}\Phi_{2,4} - \Phi_{3,4}} \tag{3.10}$$

This procedure can be repeated until no further change can be achieved with it. Then the algorithm has converged to the initial conditions of a closed orbit. It should be mentioned, that this can not be reached with random initial values for the initial condition. The initial guess has to be *close* to the condition for a DRO. Otherwise the algorithm runs the risk to converge to a different planar repeating orbit like a Lyapunov orbit about one of the linear Lagrange points, orbits about the primary, or prograde orbits about the secondary, and it can also not converge at all. To come up with a reasonable initial guess, [24] made a well-working proposal: starting with a DRO very close to the secondary (far inside the sphere of influence of the secondary), the initial guess corresponds to the velocity of a circular orbit in a two-body system. This velocity undergoes the previously mentioned algorithm to get to a more precise value. Then, an orbit slightly further away from the secondary is chosen with an initial velocity that is equal to the one of the previously calculated DRO. The algorithm to get the exact initial velocity is used again. Like this, the radius of the orbit is increased bit by bit, until the requested orbit size is reached. This method is called continuation. It should further be noted that this works independently from the choice of the starting location: the propagation can started on the primary facing side of the secondary as well as the primary averted side.

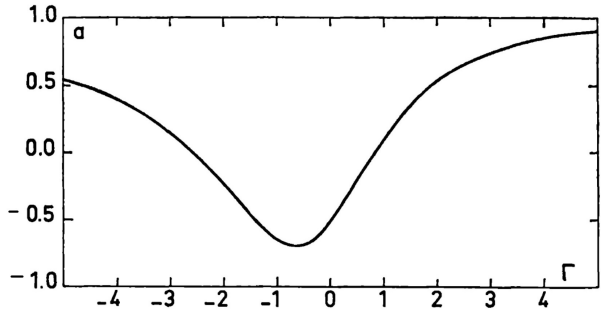

Figure 3.1: Stability index a depending on Jacobi integral Γ. [20]

3.2. Stability

Hénon, who was the first to find DROs in [20], also pointed out that this is the only group of symmetric periodic orbits that is stable no matter the orbit size (except for some rare exceptions that occur for very specific orbit sizes only). The stability index as Hénon uses it combines all eigenvalues of the monodromy matrix into one quantity for which the same rule applies as for the eigenvalues themselves: If the stability index is between -1 and 1, a closed orbit can be called stable. As can be seen in Figure 3.1, this is the case for all DROs that have been analyzed (and in fact, Hénon pointed out that 1 is the limit case for $\Gamma \to \pm\infty$). It should be mentioned that his calculations use the Hill problem and not the CR3BP, which means one of the assumptions made is that the secondary and the third body are *close*.

In case the mass fraction μ gets too large, the simple-periodic retrograde orbits can get unstable as pointed out in [2]. However, general non-periodic orbits (the difference between periodic and non-periodic DROs is explained in the next section) exist even for these large mass fractions μ. For DROs in the Earth-Moon system, [37] pointed out that even though the Sun's gravitational perturbation destroys the theoretical concept of stability, DROs will still be stable for "a long time". In fact, the simulations in [46] suggest that DROs in the Earth-Moon system can still exist for more than $10\,000$ lunar periods. Incorporating even more perturbations, [54] comes to the conclusion that Earth-Moon-resonances have to be exploited in order to obtain stable DROs. Investigations of Bezrouk and Parker in [4, 5] recommend certain orbit sizes in order to neither get pulled towards the Moon by the Moon's tides nor get distracted by the Sun's gravity field. The stability of DROs in the Jupiter-Europa system is confirmed with similar methods in [30] and [35].

3.3. Stability Regions

Before dealing with stability regions of DROs, the different types of DROs should be explained. A *periodic DRO* is the exact repeating orbit whose initial conditions can be computed as described in Section 3.1. Small changes to that result in an orbit that will still be retrograde about the secondary and therefore still be a DRO, but it is not periodic since the state after one revolution is not the exact state that the revolution has been started with. This is called a *quasi-periodic DRO*. Finally, as a special type of quasi-periodic DROs, *period-3 DROs* are DROs whose state repeats itself after exactly three revolutions. These three types of DROs can be seen in Figure 3.2.

The stability regions of DROs can be analyzed with the help of Poincaré maps. A Poincaré map shows the state for each time that the trajectory crosses a predefined subset of the state. Figure 3.2 shows three different orbits that are all DROs in the Earth-Moon system. Whenever the condition $y = 0$ is met, one point is drawn in Figure 3.3. The underlying system that has been used for this simulation is the planar CR3BP. Therefore, four variables are needed to define a state. One is given by the condition $y = 0$, two can be read from Figure 3.3 and the fourth is given with the Jacobi constant of all depicted orbits being $C = 2.91$, from which the velocity $\dot{y}$ can be calculated. Now, that the periodic DRO is stable implies that there are no (stable or unstable) manifolds for it. The period-3 DRO on the other hand is not stable and does have stable and unstable manifolds which can also be seen in Figure 3.3. The actual trajectories can be seen in Figure 3.4.

Figure 3.3 shows that the period-3 DROs in the Poincaré map are the corners of two triangles (one for the close side and one for the far side of the Moon). The triangles' edges are formed by the stable and unstable manifolds of the period-3 DROs which extend further than the triangles' corners (which is where the stable manifolds enter and the unstable manifolds leave the period-3 DRO). The interior of the triangles is the stability region for (quasi-periodic) DROs with the one periodic (period-1) DRO being in its middle.

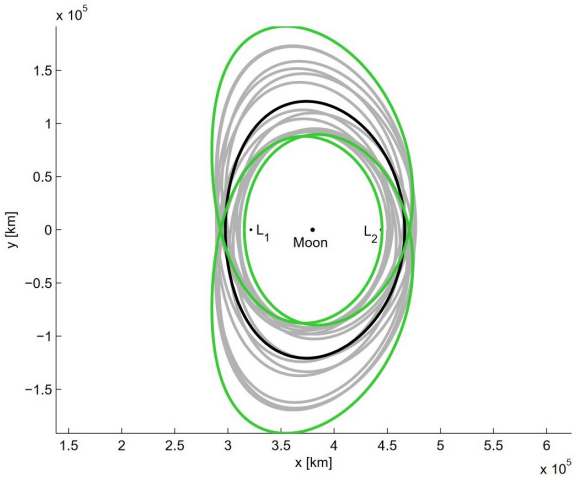

Figure 3.2: Periodic DRO (black), quasi-periodic DRO (grey), and period-3 DRO (green) in the Earth-Moon system. All orbits have the same Jacobi constant $C = 2.91$. [11]

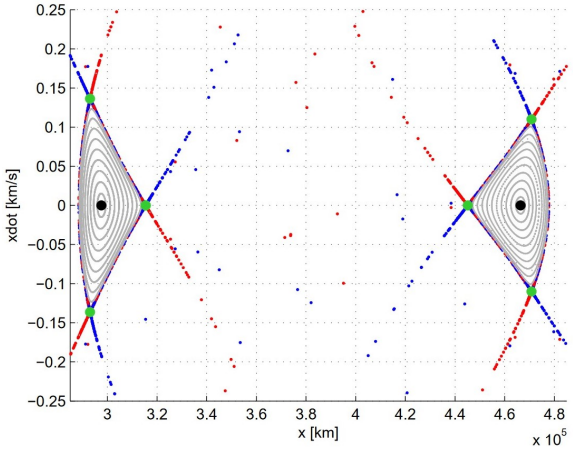

Figure 3.3: Poincaré map at $y = 0$ with periodic DRO (black), quasi-periodic DROs (grey), period-3 DRO and stable (blue) and unstable (red) manifolds of the period-3 DRO in the Earth-Moon system. All orbits have the same Jacobi constant $C = 2.91$. [11]

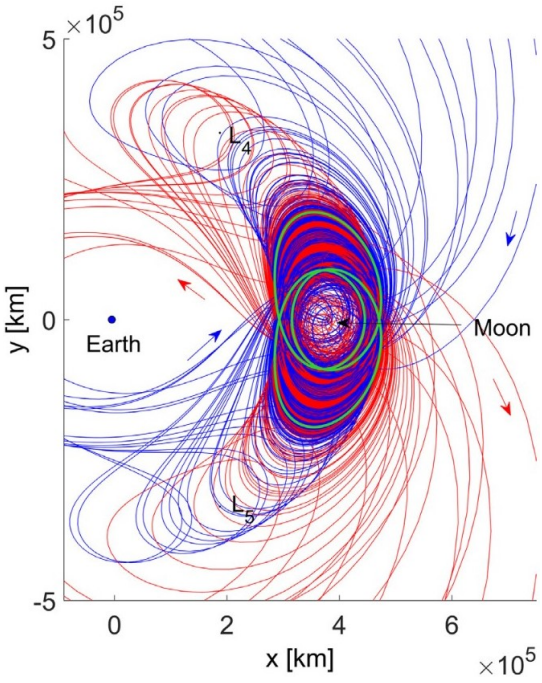

Figure 3.4: Stable (blue) and unstable (red) manifolds of the Earth-Moon period-3 DRO with $C = 2.91$. [10]

4

Modeling of Distant Retrograde Orbits

DROs are the result of the CR3BP or the Hill problem in the simplest case and the result of the forces of an unlimited number of bodies, radiation, irregular gravity, and so on in the most complex case. Therefore, in order to efficiently use DROs, it would be beneficial to model them in a straightforward way. The already existing modeling methods are presented in this chapter.

4.1. Fourier Series

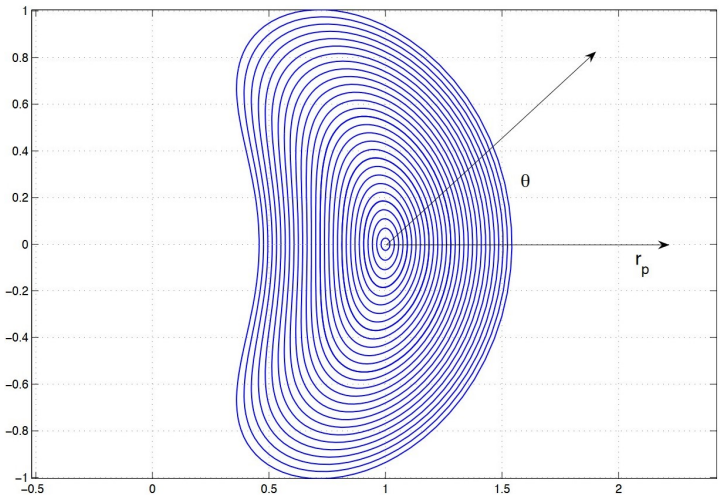

Figure 4.1: Parameters r_p and θ for several DROs with the same fixed mass ratio μ. [24]

An approach to model DROs with Fourier series has been made in [24]. It uses the CR3BP with a fixed parameter μ. A big number of DROs is numerically generated as described in Section 3.1. An orbit is parameterized with the angle θ between the x-axis and the line from the origin to the third body, as can be seen in Figure 4.1. The orbit size is defined by the distance r_p it has to the secondary when crossing the x-axis in negative y-direction. Then, the x and y coordinates are modeled as Fourier series with respect to the angle θ ([24], Equation (6)):

$$x(r_p,\theta) = \frac{a_0(r_p)}{2} + \sum_{n=1}^{\infty} a_n(r_p)\cos(n\theta) \qquad \text{and} \qquad y(r_p,\theta) = \sum_{n=1}^{\infty} b_n(r_p)\sin(n\theta) \qquad (4.1)$$

Due to the symmetry of DROs with respect to the x-axis, $x(r_p,\theta)$ does not contain sine terms and $y(r_p,\theta)$ does not contain cosine terms. For the 256 different values of r_p that were numerically propagated in [24], the coefficients $a_n(r_p)$ and $b_n(r_p)$ are calculated using the definition of Fourier series ([24],

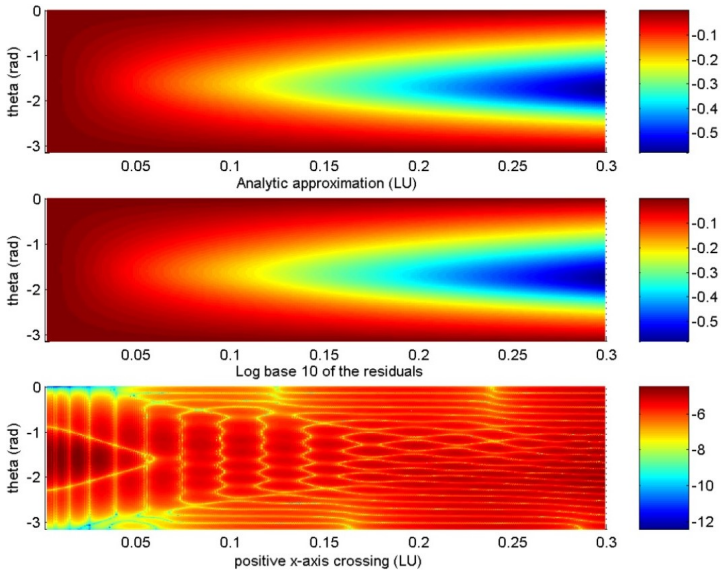

Figure 4.2: y-coordinate (color) depending on r_p (horizontal axis) and θ (vertical axis). The top plot shows the result of the numerical simulation, the second plot shows the result of the approximation with Fourier series. The third plot shows the difference between the simulation and the approximation in a $\log 10$-scale. The Fourier series is truncated after 50 terms and the Chebyshev polynomials are used up to degree 100. $\mu = 2.528 \cdot 10^{-5}$ as it is approximately the case in the Jupiter-Europa system. The Jupiter-Europa distance is about $671\,100$ km ([56], Table B.7) which is equivalent to one unit on the r_p-axis. [24]

Equation (7)):

$$a_n\left(r_p\right) = \frac{2}{\pi}\int_0^{\pi} x\left(r_p,\theta\right)\cos\left(n\theta\right)\ \mathrm{d}\theta \qquad \text{and} \qquad b_n\left(r_p\right) = \frac{2}{\pi}\int_0^{\pi} y\left(r_p,\theta\right)\sin\left(n\theta\right)\ \mathrm{d}\theta \tag{4.2}$$

The integral is approximated using the trapezoidal rule for integral estimations. The continuous functions $a_n(r_p)$ and $b_n(r_p)$ between the 256 estimated values are modeled with the use of Chebyshev polynomials. As a first result, the comparison between the numerical propagation and the estimation with the scheme described here can be seen in Figure 4.2. It is apparent that the approximation works well since the largest difference between approximation and simulation is about 10^{-5}. However, many terms had to be evaluated in order to obtain the accuracy given in Figure 4.2, since the Fourier series uses 50 terms and the Chebyshev polynomials 100.

For obtaining also the velocity, there are two options. Firstly, one can set up another two Fourier series similar to Equation (4.1) that aim to model $\dot{x}(r_p,\theta)$ and $\dot{y}(r_p,\theta)$. Secondly, the magnitude of the velocity can be obtained from the position with the Jacobi constant (see Section 2.3.2). The direction of the velocity follows from taking the derivatives of Equation (4.1) with respect to θ.

The motivation for Hirani and Russell to investigate modeling options [24] is the absence of an analytical solution for DROs. Therefore, a DRO can only be described at the discrete points to which it has been numerically propagated. This makes mission design and in particular the planning of transfers to and from DROs complicated. This Fourier model is continuous in θ and r_p and therefore allows for obtaining orbital states more efficiently and thus can help in mission planning.

4.2. Lindstedt Series

The modeling of DROs in the Hill problem case has been analyzed by Michel Hénon [20, 21], Daniel Benest [3], Martin Lara [32–34], and Masaya Kimura [26]. Among these, the analysis of Martin Lara is the most extensive one and will briefly be discussed here as well as the analysis of Daniel Benest upon which it builds. It should be noted first, that the Hill problem – with its assumptions described in Section 2.4 – assumes a short distance between the secondary and the third body. Therefore, the Hill problem is only applicable in a very limited way. The difference between DROs in the Hill problem and in the CR3BP can be seen in Figure 4.3. Because the Hill problem uses simplified equations of

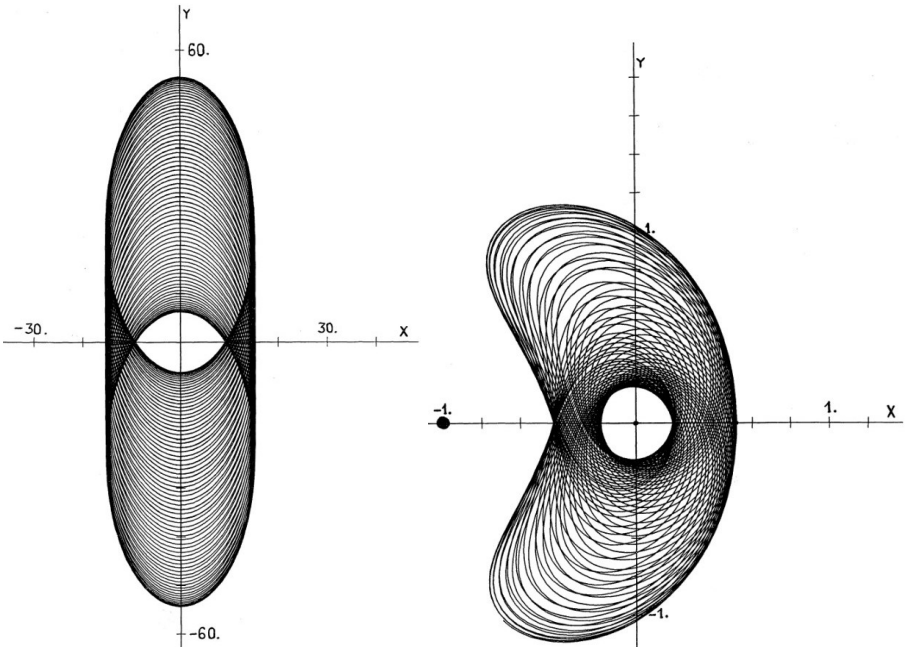

Figure 4.3: Depiction of DROs in the Hill problem case (left) and in the CR3BP (right). The coordinate axis are scaled as described in Chapter 2 and are both centered at the secondary. [3]

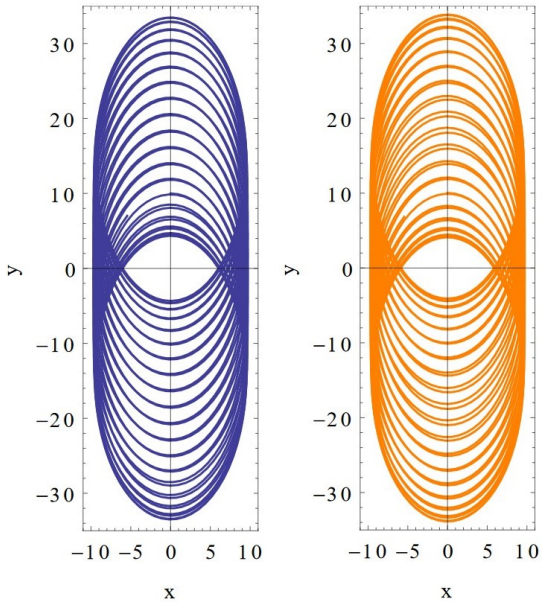

Figure 4.4: Comparison of the analytical solution (right) and the Lindstedt approach (left). The initial conditions are $x = 0$, $y = 10$, $X = -0.5$, and $Y = -0.1$. [32]

motion with respect to the CR3BP, also the solution is of simpler shape. In fact, it can be modeled quite well as an elliptical motion with the center of the ellipse librating about the secondary. If the mutual attraction between secondary and third body in the Hill problem is neglected, the equations of motion reduce to the *Clohessy-Wiltshire equations* (CW-equations) [12]; equations that are used for example for the relative motion of satellites and rendezvous. These CW-equations expressed in the coordinate system of the Hill problem are, when omitting the third dimension:

$$\ddot{\xi} = 2\dot{\eta} + 3\xi \qquad \text{and} \qquad \ddot{\eta} = -2\dot{\xi} \tag{4.3}$$

This is exactly the same as the Hill equations (Equation (2.46)) except for the gravitational attraction between the secondary and the third body is missing. The CW-equations can be solved analytically and yield an ellipse that is potentially drifting in η-direction:

$$\xi = A\cos t + B\sin t + 2C \qquad \text{and} \qquad \eta = -2A\sin t + 2B\cos t - 3Ct + D \tag{4.4}$$

A, B, C, and D are scalar constants. The ellipse has a semi-minor axis of $\sqrt{A^2 + B^2}$ in ξ-direction and a semi-major axis of $2\sqrt{A^2 + B^2}$ in η-direction. At time $t = 0$, its center is $2C$ in ξ-direction and D in η-direction away from the secondary. The ellipse is moving with the velocity $3C$ in negative η-direction. Now adding the attraction between the secondary and third body yields the Hill equations which can not be solved analytically. After Daniel Benest found a quite good approximation for the movements of the center of the ellipse, Martin Lara made a good attempt of analytically modeling these using Hamiltonians.

As mentioned in Section 2.4.3, the Hamiltonian $\mathcal{H}$ for the Hill problem is:

$$\mathcal{H} = \underbrace{\frac{1}{2}(X+y)^2 + \frac{1}{2}(Y-x)^2 - \frac{3}{2}x^2}_{\text{Clohessy-Wiltshire}} \underbrace{- \frac{1}{\sqrt{x^2+y^2}}}_{\text{mutual attraction}} \tag{4.5}$$

It consists of the Clohessy-Wiltshire part, that – as mentioned previously – has an analytical solution, and the mutual attraction term for the gravitational attraction between the secondary and third body. The following change in coordinates from (x, y, X, Y) to (ϕ, q, Φ, Q) enables the analytical integration of the CW-part (as found in [32] with $\omega = 1$):

$$x = b\,(2\xi + \sin\phi)\,, \qquad y = 2b\,(\eta + \cos\phi)\,, \qquad X = -b\,(2\eta + \cos\phi)\,, \qquad Y = -b\,(\xi + \sin\phi) \tag{4.6}$$

with

$$b = \sqrt{2\Phi}, \qquad \xi = \frac{Q}{2kb}, \qquad \text{and} \qquad \eta = \frac{kq}{b}, \tag{4.7}$$

of which b and ξ happen to be constant (see Equation (4.11)). b, ξ and η are parameters of the orbit itself while k on the other hand is a scalar property of the coordinate change that can be chosen arbitrarily. Now, the CW-part of the Hamiltonian $\mathcal{H}$ from Equation (4.5) simplifies to:

$$\mathcal{H} = \Phi - \frac{3}{8}\left(\frac{Q}{k}\right)^2 \tag{4.8}$$

Then, according to the rules of Hamiltonian dynamics, the rates of change for the coordinates ϕ, q, Φ, and Q can be calculated as follows:

$$\dot{\phi} = \frac{\partial \mathcal{H}}{\partial \Phi} = 1, \qquad \dot{q} = \frac{\partial \mathcal{H}}{\partial Q} = -\frac{3}{4k^2}Q, \qquad \dot{\Phi} = -\frac{\partial \mathcal{H}}{\phi} = 0, \qquad \dot{Q} = -\frac{\partial \mathcal{H}}{\partial q} = 0 \tag{4.9}$$

For the sake of simplicity, k is chosen to be:

$$k = \frac{\sqrt{3}}{2} \tag{4.10}$$

Therefore:

$$\phi(t) = \phi_0 + t, \qquad q(t) = q_0 - Q_0 t, \qquad \Phi(t) = \Phi_0, \qquad Q(t) = Q_0 \tag{4.11}$$

Inserting Equations (4.7), (4.10) and (4.11) in Equation (4.6) corresponds to the findings from Equation (4.4) (when considering that ξ and η in Equation (4.4) refers to x and y in Equation (4.6)). Now, including the mutual attraction term in the Hamiltonian $\mathcal{H}$, it can be written as ([32], Equations (14) to (17)):

$$\mathcal{H} = \Phi\left(1 - 3\xi^2 - \frac{1}{\sqrt{8\Phi^3}\sqrt{1 - k^2\sin^2\phi + \xi\sin\phi + 2\eta\cos\phi + \xi^2 + \eta^2}}\right) \tag{4.12}$$

In order to solve this Hamiltonian, the second of the square roots is expanded in a power series using Lindstedt series as defined in [41]. Their exact definition is beyond the scope of this text. The result of the further analysis can be seen in Figure 4.4. It compares the analytical result with the result using Lindstedt series. This is done with initial conditions that yield a strongly librating orbit. It can be seen that the approximation given by the Lindstedt series works well and is able to reproduce all of the major features of the orbit. On the other hand, it has to be noted that this model is little flexible when it comes to small changes: perturbing forces can not easily be incorporated as well as a potential stability analysis or three dimensional orbits. In addition to that – as stated in the beginning – the Hill problem is only a good approximation of the CR3BP when assuming a very close distance between the secondary and the third body.

4.3. Conclusions

First, it should be noted that these two models described above try to achieve different things. While the Fourier Series approach deals with closed, repeating DROs, the Lindstedt Series approach deals with DROs that do not meet the exact initial conditions to be closed, repeating DROs, but rather quasi-periodic DROs. Furthermore, the Fourier Series deal with the CR3BP while the Lindstedt Series take place in the Hill problem. The two models are both useful in some cases. The Fourier Series approach can be used for evaluating transfer options, since it can give the velocity vector of a DRO depending on the position in an efficient way without many calculations. The Lindstedt Series are useful for analyzing the libration of DROs in the Hill problem case – although the Hill problem is of limited use for real three-dimensional analysis. Therefore, a modeling technique that allows for more flexibility, that can take quasi-periodic DROs, and potentially even perturbing forces into account, and that does not make use of the simplifying assumptions of the Hill problem, is desired.

5

Transfer to Distant Retrograde Orbits

The transfer to a DRO can happen from different original locations. This depends on where the DRO is located (for example in the Sun-Earth system or the Earth-Moon system) and what the application is. A DRO about the Moon in the Earth-Moon system for example can be beneficial for a future space hub, aimed to refill spacecraft coming from Earth on the way to other Solar System bodies. The base of the space hub can be an asteroid that has been brought in an Earth-Moon DRO in order to be mined and to serve as this kind of space hub. This means, there are transfers from Earth (the primary) and from the outside of the Earth-Moon system involved. The third option is a transfer from the secondary to the DRO. An application for this transfer can be found for example in space observation instruments, that need to be outside the Earth's magnetic field but should remain in the vicinity of Earth. Those could be placed on DROs in the Sun-Earth system about the Earth(-Moon system). Then, a transfer from Earth (the secondary) is necessary to reach this orbit.

Multiple attempts have been made already to come up with transfers in these different scenarios, some of them are presented in the next sections.

5.1. From Primary

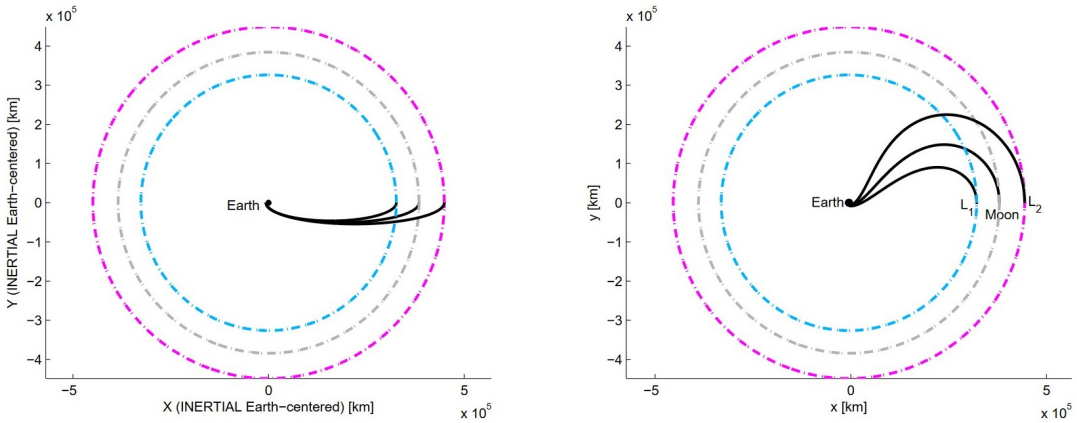

Figure 5.1: Hohmann transfers from Earth to Moon, L1, and L2 in an inertial coordinate system (left) and in a rotating coordinate system (right). [11]

A transfer from the primary to the DRO is the most analyzed transfer option in literature, since it is (among others) represented by a transfer from Earth to a Moon DRO. Lucia Capdevila [10, 11] has modeled this with the following simple approach: from a (prograde) Low Earth Orbit (LEO), the spacecraft accelerates in the direction of motion in order to enter a transfer orbit that brings it further away from Earth. Its nearly elliptic shape as seen in an inertial reference frame is perturbed only by the gravity field of the Moon. As can be seen in Figure 5.1, when converting the trajectory into a rotating

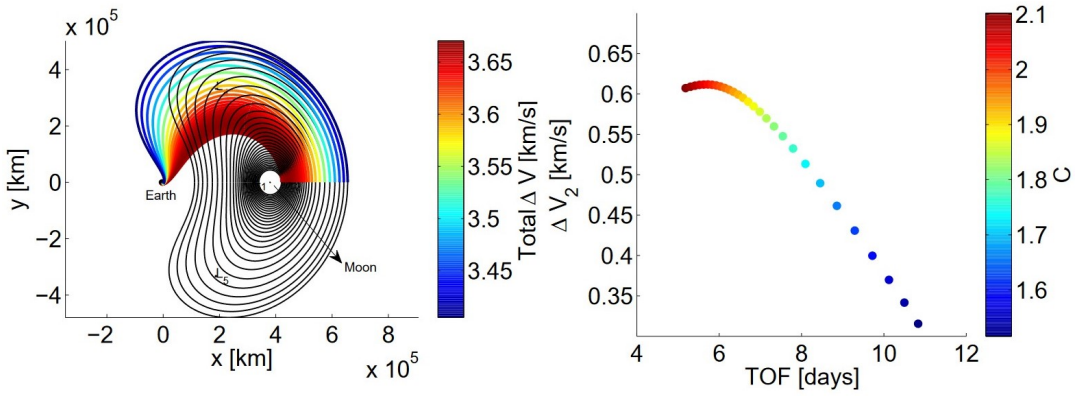

(a) Geometry and total ΔV (b) ΔV_2, TOF, and transfer Jacobi constant, C

Figure 5.2: Overshooting Hohmann-like transfers from Earth to Moon DROs, in the rotating coordinate system and the needed ΔV (left) and their times of flight (TOF) and their Jacobi constants (right). [11]

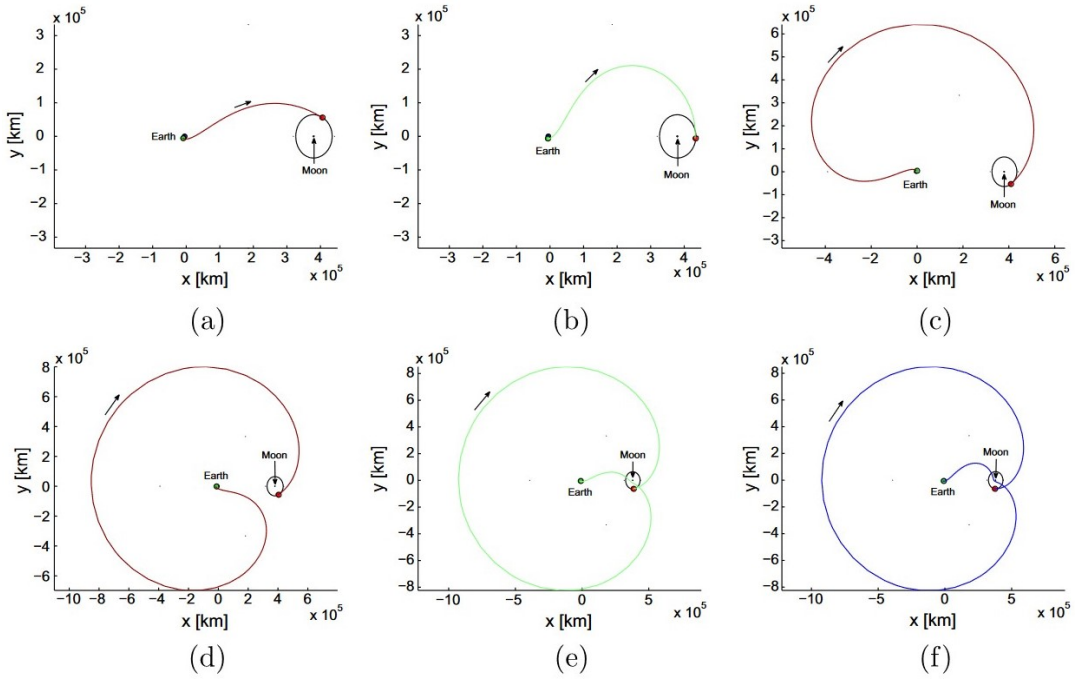

Figure 5.3: Different transfers from Earth to Moon DROs of fixed size, in the rotating coordinate system. [10]

coordinate system, the Hohmann trajectory is bent towards the Moon. Now, all Hohmann-like trajectories (Hohmann-like because the Moon's gravity *does* play a role, therefore the trajectory is not a perfect Hohmann transfer), that "overshoot" the Moon, are tangential to one of the DROs, meaning the DRO can be accessed by accelerating along the direction of motion. This can be seen in Figure 5.2, where for some DROs of different size this Hohmann-like transfer with two impulsive shots – one in LEO and one on the other side of the Moon – is depicted.

In a real scenario, the desired DRO size is given and the location of the second maneuver is not restricted to be exactly behind the Moon. In this case, not the orbit size but the time of flight is one possible parameter of the transfer. This type of transfer is named "family A" in [10] and some of their orbits are depicted in Figure 5.3. These orbits can easily be analyzed in terms of ΔV and time of flight. More complex transfers that include Moon flybys are possible and can be beneficial depending on the situation.

Some other research is briefly mentioned here: Tan Minghu [38] points out that it can be beneficial for the ΔV-budget to enter a Lyapunov orbit abound the Sun-Earth Lagrange point L1 or L2 on one of their stable manifolds and to leave it on an unstable manifold that is connected to the desired Moon DRO. Of course this transfer comes with a high time of flight. Chelsea Welch [57] shows that a Moon flyby on the far side of the Moon usually results in ΔV savings compared to a direct transfer and also compared to a transfer with a flyby on the close side of the Moon. This is in line with the findings of Lucia Capdevila and Naomi Murakami [40].

5.2. From Secondary

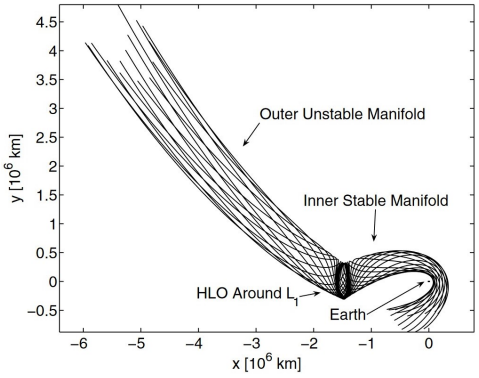

Figure 5.4: Outer unstable and inner stable manifold of L1 Lyapunov orbit in Sun-Earth system. [14]

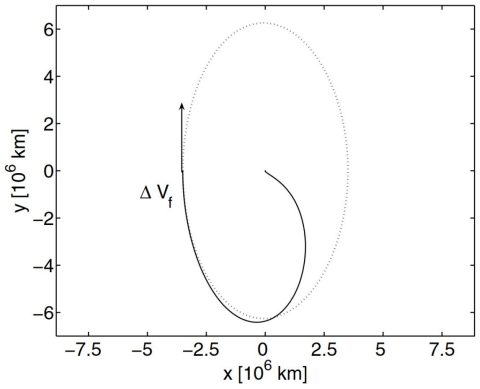

Figure 5.5: Lyapynov transfer (solid line) from Earth (origin) to Sun-Earth DRO (dotted line). [14]

In the most cases of interest, a transfer from the secondary to a DRO is a transfer from Earth to a DRO in the Sun-Earth system. The traditional approach for this transfer can – according to Jacob

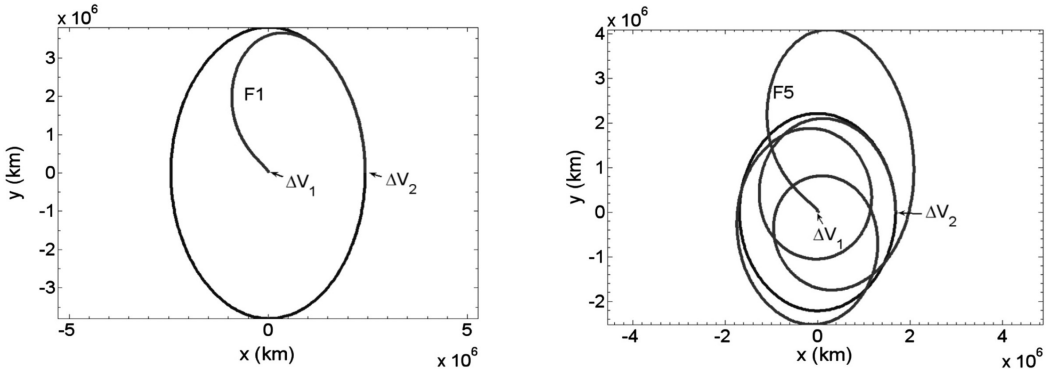

Figure 5.6: Transfer options “F1” (left) and “F5” (right) from Earth to Sun-Earth DRO. [50]

Demeyer [14, 15] – be found in [44]: for any given DRO that extends further than the Lagrange point L1, there is a L1 Lyapunov orbit tangential to it at the x-axis. Therefore, after reaching the Lyapunov orbit, an impulsive shot in the direction of motion is needed to enter the DRO. To reach the Lyapunov orbit, its stable manifolds can be followed. This is in particular useful, since those manifolds get very close to the secondary, which can be seen in Figure 5.4 for the Sun-Earth system. One of these Lyapunov transfers is depicted in Figure 5.5. Since it is not necessarily the case that a stable manifold meets the LEO parking orbit tangentially, a differential corrector can be applied to correct for this discrepancy (read [14], Section III.). For small DROs (for the Sun-Earth system DROs with semi-minor axis smaller than $4 \cdot 10^6$ km) this method can be adapted to obtain smaller ΔV-values.

Christopher Scott [49–51] analyzed the phase space of DROs with Poincaré maps. Among other insights, this also resulted in five different transfer classes from Earth to Sun-Earth DROs. Of those classes, in terms of transfer time, the class “F1” always outperforms the others, while in terms of total ΔV class “F5” is better than the other classes for most of the DRO sizes. Those two orbits can be seen in Figure 5.6. It is apparent, that class “F1” has big similarities with the Lyapunov transfer from Figure 5.5.

The transfer between a DRO and a secondary is also analyzed by Ruikang Zhang [58], although he focuses on the opposite scenario: a transfer from an Earth-Moon DRO to a Low Lunar Orbit (LLO). As one of very few authors he therefore also considers three-dimensional transfers and the perturbing influence of the Sun’s gravitation.

5.3. From Outside

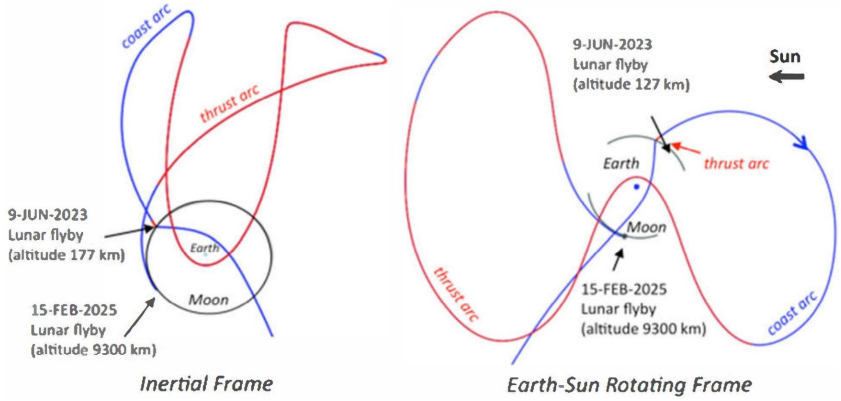

Figure 5.7: Capturing an asteroid in a Moon orbit in an inertial reference frame (left) and an Earth-Sun rotating frame (right). Taken from [39], Figure 5.

The least researched transfer is the one between a DRO and the outside of the considered two-body system (also a large orbit around the primary can be considered as *outside*). This is particularly

remarkable, since for capturing an asteroid in an Earth-Moon DRO, this is exactly the transfer that is needed. And yet, the astrodynamical specifics of this kind of mission have not been investigated in detail. [39] offers a first idea of how this could look like, which can be seen in Figure 5.7. Due to the impossibility of impulsive shots, the analysis of an asteroid retrieval mission is more complex than when considering a spacecraft transfer.

Collin Bezrouk [6] for example analyzed the transfer of a spacecraft that is in a Mars orbit for reaching a Mars-Phobos DRO. This is especially challenging, since Phobos has a very weak gravitational field and an irregular shape. Therefore, a self-set requirement in this paper is to not have a maneuver close to Phobos.

The absence of further investigations on this topic enables to think about future research. Especially since a potential asteroid will likely be brought in a DRO, the exact transfer has yet to be determined. Furthermore – in case this asteroid or a human-made space station in an Earth-Moon DRO is in fact used as a space hub – transfer possibilities for spacecraft to leave the Earth-Moon system from this DRO have to be established.

6

Propagation and Integration

Simulating DROs and transfers to them is a crucial part of the investigations. This does not not only hold for the case that the research question will be answered mainly with simulations. Even in case the thesis turns out to be rather analytical, simulating the results is a mandatory part of the verification and validation process. For the simulation itself, certain choices have to be made. These are made here exemplary for two different kinds of simulations that can be expected in the thesis. Therefore, the DRO will be restricted to be an Earth-Moon DRO. Although other DROs are commonly investigated as well – especially Sun-Earth DROs –, the Earth-Moon DROs promise the most useful applications and their first execution is likely to be in the near future. The two considered examples are explained in the next section followed by a section treating the propagator choices and a section about the integrator choices.

6.1. Simulation Scenarios

For Earth-Moon DROs, two main simulations can be distinguished. Firstly, an object that is in a DRO whose long-term evolution is to be analyzed. Secondly, a transfer to a DRO. These two options are very different in one main aspect which is the total time of the simulation. While a transfer is not supposed to take more than some months (if coming from Earth) or some years (when coming from outside the Earth-Moon system), the analysis of the long-term evolution is typically done over a period of thousands of years. Therefore it is justified to use two different sets of propagation and integration settings.

6.2. Propagator

Propagator refers to a set of variables that can be chosen for the propagation. Typically, for propagating the motion of one spacecraft, six variables (three position and three velocity variables in three-dimensional space) are needed for this. A propagator with which most of the variables do not undergo big changes throughout the propagation process is desired. This minimizes the round-off errors and the computation time.

6.2.1. Cowell Propagator

The Cowell propagator is the most straightforward and therefore simplest propagator scheme. A state $\mathbf{S}$ is represented by three position and velocity components in an inertial Cartesian coordinate system:

$$\mathbf{S} = \begin{bmatrix} x & y & z & \dot{x} & \dot{y} & \dot{z} \end{bmatrix}^{\mathsf{T}} \tag{6.1}$$

With the forces $\mathbf{F}$ acting on the body being explained in Section 2.1, the derivative of the state $\mathbf{S}$ can be calculated using their sum $\Sigma\mathbf{F}$ and the body's mass m:

$$\dot{\mathbf{S}} = \begin{bmatrix} \dot{x} \\ \dot{y} \\ \dot{z} \\ \ddot{x} \\ \ddot{y} \\ \ddot{z} \end{bmatrix} = \begin{bmatrix} \dot{x} \\ \dot{y} \\ \dot{z} \\ \Sigma F_x/m \\ \Sigma F_y/m \\ \Sigma F_z/m \end{bmatrix} \tag{6.2}$$

The obvious disadvantage of the Cowell propagator is that all of the six parameters change within their entire (maximal useful) range during one revolution. Therefore, for most of the problems it is desired to work with a more suitable propagator than the Cowell propagator.

6.2.2. Kepler Elements Propagator

The Kepler elements propagator makes use of the Kepler elements that have been defined in Section 2.2. The state $\mathbf{S}$ consists of the Kepler elements *semi-major axis* a, *eccentricity* e, *inclination* i, *right ascension of the ascending node (RAAN)* Ω, *argument of periapsis* ω, and one of the anomalies *true anomaly* θ, *mean anomaly* M and *eccentric anomaly* E:

$$\mathbf{S} = \begin{bmatrix} a & e & i & \Omega & \omega & M \end{bmatrix}^{\mathsf{T}} \tag{6.3}$$

If the object is in an unperturbed orbit about a central mass, the anomaly will be the only parameter that experiences change during one revolution. Therefore, – if the orbit can be approximated well with a Kepler orbit – five out of the six parameters are changing only slightly or not at all. This does not apply to DROs: DROs are typically in a state between "orbiting the secondary with perturbations from the primary" and "orbiting the primary with perturbations from the secondary". Very small DROs can be modeled well as orbiting the secondary while extremely large DROs can be seen as highly eccentric orbits abound the primary. For all other DROs – no matter if the primary or the secondary is chosen as central mass – the advantages of using Kepler elements are defeated by this. The use of Kepler elements for DROs therefore has to be considered carefully.

Kepler elements have another disadvantage which is more general and not referring to DROs: Kepler elements do have singularities. Firstly, this occurs for perfect circular orbits with zero eccentricity $e = 0$, since then periapsis and thus the argument of periapsis ω is not defined properly. This also asks for a redefinition of the anomaly which is usually defined as the (true/mean/eccentric) angle that has passed since the last periapsis. Secondly, prograde equatorial ($i = 0$) and retrograde equatorial ($i = \pi$) orbits do not have an ascending node and therefore the right ascension of the ascending node Ω is undefined. Finally, for an eccentricity of 1 which corresponds to a parabolic orbit, the semi-major axis a is undefined.

6.2.3. Encke Propagator

The idea of the Encke propagator is that a perturbed orbit will evolve – at least for a limited time after initial time t_0 – closely to the Kepler orbit that corresponds to the state at t_0. The evolution of the Kepler orbit can be solved analytically (see Section 2.2), while the true orbit $\mathbf{r}$ experiences the additional force $\mathbf{a}_{\text{pert}}$. Then, the difference $\boldsymbol{\rho}$ evolves according to [18] as:

$$\Delta\ddot{\mathbf{r}} = \frac{\mu}{\rho^3}\left(\mathbf{r}\mathcal{F}(q) - \Delta\mathbf{r}\right) + \mathbf{a}_{\text{pert}} \tag{6.4}$$

with

$$q = \frac{1}{2}\left(\frac{r^2}{\rho^2} - 1\right) \qquad \text{and} \qquad \mathcal{F}(q) = \frac{2q}{1+2q}\left(1 + \frac{1}{1+2q+\sqrt{1+2q}}\right) \tag{6.5}$$

The advantages compared to the Cowell Propagator are the smaller values that the state and the state derivative assume. On the other hand, the Encke propagator has to be "restarted" after a while, when the Kepler orbit and the real orbit differ too much.

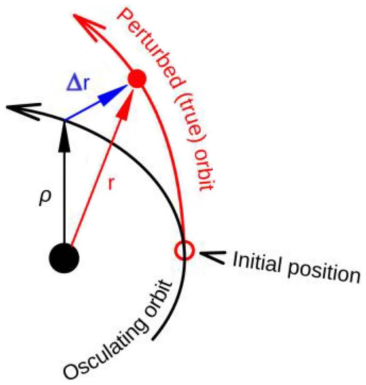

Figure 6.1: Concept sketch of the Encke propagator with the position $\boldsymbol{\rho}$ on the Kepler orbit, the position $\mathbf{r}$ on the true orbit and the difference $\Delta\mathbf{r}$ between them. [18]

6.2.4. Modified Equinoctial Elements Propagator

The Modified Equinoctial Elements (MEE) aim to get rid of the three different singularities that the Kepler elements have. This is achieved by using slightly adapted parameters. According to [18], the seven parameters are:

$$p = \begin{cases} a\left(1-e^2\right) & e \neq 1 \\ 2a & e = 1 \end{cases} \tag{6.6}$$

$$f = e\cos\left(\omega + I\Omega\right) \qquad \text{and} \qquad g = e\sin\left(\omega + I\Omega\right) \tag{6.7}$$

$$h = \tan^I\left(\frac{i}{2}\right)\sin\left(\Omega\right) \qquad \text{and} \qquad k = \tan^I\left(\frac{i}{2}\right)\cos\left(\Omega\right) \tag{6.8}$$

$$L = \omega + I\Omega + \theta \qquad \text{and} \qquad I = \pm 1 \tag{6.9}$$

Here, p is the semi-latus rectum which is well defined for all Kepler orbits including parabolic ones. f and g combine the eccentricity e and the position of the periapsis. If the orbit is circular and the position of the periapsis is thus undefined, they are simply 0. h and k combine the inclination i with the right ascension of the ascending node Ω. For non-inclined orbits they are both zero (if I is chosen correctly). The parameter L is the one parameter that will change within a Kepler orbit and is the only parameter that undergoes large changes in a perturbed orbit. The definitions of these six parameters do not require the parameter I. They are properly defined with using $I = 1$. However, in this case one of the singularities still exists: for retrograde equatorial orbits the parameters h and k require $\tan(\pi/2)$ – which is not properly defined. On the other hand, if I is chosen to be -1, this problem arises for prograde (and only prograde) equatorial orbits. The solution is to change the parameter I (a so-called shadow parameter) whenever it comes to close to an equatorial orbit and I has not already the suiting value. In most cases this does not happen very often since it requires the orbit to switch between prograde and retrograde and to be close to equatorial afterwards.

6.2.5. Unified State Model Propagator and Derivatives

The Unified State Model (USM) [55] is as the MEE free of singularities, if a seventh shadow parameter is used. The USM uses three parameters to determine size and shape of the current Kepler orbit that are obtained with a velocity hodograph. The orientation is – again, as for the MEE – determined with three parameters and one shadow parameter. Alternative formulations allow the use of quaternions or Rodrigues parameter. Using quaternions means having four full parameter instead of three parameters and one shadow parameter.

6.2.6. Comparison

In conclusion it can be said that the Cowell propagator is the “brute force” approach to simulate an orbit. It works always but the big changes that all of the six parameters experience during one revolution make it slow and prone to integration errors. The Kepler elements propagator is the first attempt to encounter this problem by having only one parameter that changes during an unperturbed orbit. However, this comes with three singularities. These are resolved in the MEEs and the USM, introducing a

seventh (shadow) parameter which is chosen to be 1 or -1 depending on the current state. Finally, the Encke propagator computes the current state as a difference to an analytically propagated Kepler orbit.

An important factor when simulating DROs is the fact that they can not be approximated well with Kepler orbits. This is because instead of orbiting one central mass and having another object perturbing the orbit, a DRO rather means orbiting two bodies at the same time. This does not hold for DROs that are very close to the secondary and whose orbits can be almost circular, and also not for DROs that are very far from the secondary and therefore orbiting the primary with the secondary being a small perturbation. But the many DROs in the wide spectrum between those two extremes do not behave as Kepler orbits with respect to either of the primaries. This defeats the advantage that the Kepler elements propagator and therefore also the MEE and the USM propagators have: it does not hold anymore that five of the elements will be constant or only slightly changing. For obvious reasons, it also defeats the purpose of the Encke propagator. Therefore, for actually simulating DROs, all of the propagators have to be analyzed in the respective situation and compared to each other in terms of computation time and accuracy. Another possibility and potential research question is to develop a new set of elements that is perfect to use for DROs.

6.3. Integrator

Once the right propagator and thus differential equation has been chosen, an integrator has to be selected. The integrators that are available in Tudat (see Section 8.1) can be found in [16]. The concept of a numerical integration method will be explained here with taking the Forward Euler method as an example. The Forward Euler is the most "primitive" integration method which usually performs badly. It should be noted first that any second-order differential equation can be reformulated to be a first-order differential equation with twice the number of variables by defining the first derivative of each of the variables as a new variable. This means, the following system of first-order differential equations needs to be solved, with $\mathbf{f}(\mathbf{S}, t)$ being a known function:

$$\dot{\mathbf{S}} = \mathbf{f}(\mathbf{S}, t) \tag{6.10}$$

The Forward Euler method now evaluates the function $\mathbf{f}(\mathbf{S}, t)$ at the current state $\mathbf{S}_i$ and adds this value, multiplied by the step size Δt to the current state $\mathbf{S}_i$:

$$\mathbf{S}_{i+1} = \mathbf{S}_i + \Delta t \mathbf{f}(\mathbf{S}_i, t_i) \tag{6.11}$$

This yields the correct result under the assumption that $\mathbf{f}$ does not change with time t or state $\mathbf{S}$, which is in general – of course – not true.

The Forward Euler method can be augmented to become the more general Runge-Kutta methods (by Runge and Kutta, [27, 47]). For these methods, more than one evaluation of $\mathbf{f}(\mathbf{S}, t)$ is necessary to determine the next state $\mathbf{S}_{i+1}$. This is compensated by being more accurate, meaning having a higher order (which is explained later). Therefore, even if the step size for a Runge-Kutta method is increased such that it needs the same number of evaluations of $\mathbf{f}(\mathbf{S}, t)$ per unit of time, it comes closer to the true (analytical) solution of the differential eq. (6.10) than the Forward Euler method. The equations for explicit Runge-Kutta methods are (implicit Runge-Kutta methods are not treated here):

$$\mathbf{S}_{i+1} = \mathbf{S}_i + \Delta t \sum_{n=1}^{s} b_n \mathbf{k}_n \tag{6.12}$$

with $\mathbf{k}_n$ being:

$$\mathbf{k}_n = \mathbf{f}\left(\mathbf{S}_i + \Delta t \left(\sum_{l=1}^{n-1} a_{n,l} \mathbf{k}_l\right), t_i + c_n \Delta t\right) \qquad \forall n \in 1, \ldots, s \tag{6.13}$$

with $a_{n,l}$, b_n and c_n being parameters of the respective Runge-Kutta method, and s the number of evaluations of $\mathbf{f}(\mathbf{S}, t)$ that is needed for one step. The most famous Runge-Kutta method, a fourth-order Runge-Kutta method (RK4) with $s = 4$, has the following parameters:

$$c_1 = 0, \qquad c_2 = \frac{1}{2}, \qquad c_3 = \frac{1}{2}, \qquad c_4 = 1, \tag{6.14}$$

$$a_{2,1} = \frac{1}{2}, \qquad a_{3,1} = 0, \qquad a_{3,2} = \frac{1}{2}, \qquad a_{4,1} = 0, \qquad a_{4,2} = 0, \qquad a_{4,3} = 1, \tag{6.15}$$

$$b_1 = \frac{1}{6}, \qquad b_2 = \frac{1}{3}, \qquad b_3 = \frac{1}{3}, \qquad b_4 = \frac{1}{6} \tag{6.16}$$

Now, regarding the order of a Runge-Kutta Method: with series expansion, the error – meaning the difference between the true solution and the estimated solution – can be approximated. This is shown with the Forward Euler as an example following [16] with using this scalar first-order differential equation:

$$\dot{y} = f\left(y, t\right) \tag{6.17}$$

Then, the estimation $\bar{y}$ after one step Δt following Forward Euler is:

$$\bar{y}\left(t + \Delta t\right) = y\left(t\right) + \Delta t f\left(y, t\right) \tag{6.18}$$

while the true solution y after one step Δt can be written with Taylor series:

$$y\left(t + \Delta t\right) = \sum_{i=0}^{\infty} \frac{\left(\Delta t\right)^i}{i!} \frac{\mathrm{d}^i}{\mathrm{d}t^i} y\left(t\right) \tag{6.19}$$

which means, for the difference it holds:

$$\bar{y}\left(t + \Delta t\right) - y\left(t + \Delta t\right) = \sum_{i=2}^{\infty} \frac{\left(\Delta t\right)^i}{i!} \frac{\mathrm{d}^i}{\mathrm{d}t^i} y\left(t\right) = \frac{1}{2}\left(\Delta t\right)^2 \dot{y}\left(t\right) + \frac{1}{6}\left(\Delta t\right)^3 \ddot{y}\left(t\right) + \ldots = \mathcal{O}\left(\Delta t^2\right) \tag{6.20}$$

Therefore, the error after one step, called local truncation error, has order two. Since the number of steps needed to cover a defined time span is indirectly proportional to the step size, the error after this defined time span (called global truncation error) has the order

$$\mathcal{O}\left(\Delta t^2\right) \cdot \frac{1}{\Delta t} = \mathcal{O}\left(\Delta t\right) \tag{6.21}$$

which is why the Forward Euler is referred to as a first-order method. Runge-Kutta methods are usually designed to have the highest order possible with a given number of function evaluations. It should be noted, that a higher order also means a higher accuracy for the same number of function evaluations if the step size Δh is small enough, since in the limit case only the order and not its factor is important. The step size can be decreased until the mathematical boundaries that are imposed by the number of digits that are used to represent the state are reached. Eventually, the rounding errors (and their accumulation and amplification over time) get bigger than the truncation error.

These Runge-Kutta methods can be used with a fixed step size, or – to further increase the accuracy per function evaluation – with a variable step size depending on "how fast" the state $\mathbf{S}$ changes. For example, in a highly eccentric orbit, when the spacecraft is close to the periapsis, more steps per time are desirable. The Runge-Kutta-Fehlberg (RKF) integrator and the Dormand-Prince (DOPRI) integrator use the difference of two different Runge-Kutta integrators to estimate the local truncation error that is made and adjust the step size accordingly to reach a previously defined target truncation error. Another way of reacting to different situations is adjusting the order of the used Runge-Kutta method instead of the step size. This is done in the Adams-Bashforth-Moulton (ABM) methods, which also incorporate previous evaluation of the function $\mathbf{f}(\mathbf{S}, t)$ to estimate the new state (for which it is called a multi-step method). Finally, the Bulirsch-Stoer (BS) methods use different step sizes at the same time and aim to extrapolate which state $\mathbf{S}$ would be reached with an infinite number of steps (an infinitesimal step size).

The question which integrator is appropriate for which situation can not be answered in a definite way, which is why the various integrators are not described in more detail here. Instead, for any given situation, the best suiting integrator has to be figured out. This can be achieved by first creating a benchmark solution with using a very small step size (optimally the rounding error and the truncation error should be the same), and then comparing different integrators (with higher step sizes than the benchmark) to the benchmark to see which one performs best.

7

Optimization

Optimization is the process of finding input and control variables, parameters, coefficients, configurations, or initial conditions that yield an optimal or close-to-optimal solution. How the quality of a solution is assessed depends on the situation and the specific goals, and is usually defined in a function called *fitness function* or *objective function*. It can combine multiple objectives to only one fitness value or it can output multiple objectives which then have to be compared and analyzed further. In this chapter, in the first section some general notes about optimization are made, followed by two sections that briefly treat the most important optimization methods.

7.1. General Notes

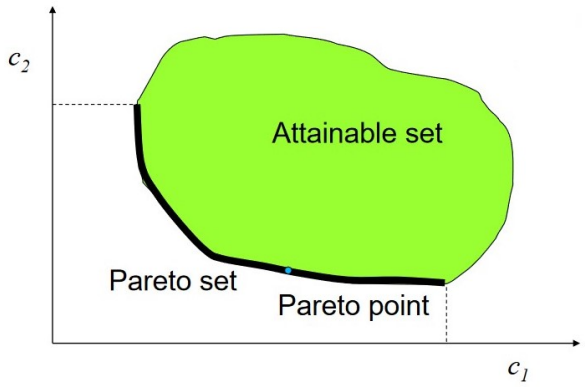

Figure 7.1: Set of reachable objectives c_1 and c_2 in green with Pareto front as a thick black line. In this example, both objectives shall be minimized. [31]

If one wants to apply an optimization to a problem, one needs to know exactly how many and which parameters can be adjusted, what their respective restrictions are, and how the objective(s) are defined. Restrictions to the variables can be applied by constraining the parameter space. For example, when designing an Earth orbit, perigee should be above the Earth's surface and depending on the application also above the Earth's atmosphere. For some methods it might not be possible to hard code parameter constraints, or the constraints are not known beforehand because they are not referring to the parameters themselves but to functions of them. In this case, the constraints can be implemented by applying a penalty value for sets of parameters that are outside the intended parameter space. This can introduce a discontinuity to the objective function which can imply the need for further adjustments of the method, depending on which optimization technique is used.

When multiple objectives exist that can not be combined into one single objective or the combined objective function is simply not specified (for example, for transfers this is typically the transfer time

and ΔV), optimization needs to be done based on the so-called *Pareto front*. The Pareto front is the result of ignoring all sets of parameters that are *for sure* worse than one of the other sets of parameters. This is given if *all* of the objectives perform worse for this specific set of parameters than for one other specific set of parameters. This is illustrated in Figure 7.1.

7.2. Global Optimization Methods

The start of every optimization is usually a global optimization. This aims to find parameters that are somehow *close* to the global optimum. This is very difficult in cases where many local optima are present.

7.2.1. Grid Search

The most trivial optimization method is grid search. It is rarely used because of its poor performance but it needs to be mentioned as the original and most straightforward method. Each of the n dimensions of the parameter space is divided into a given number of equally spaced points and finally every point in the grid is evaluated on its own. Regions with good objective values are not investigated in more detail than regions with bad objective values. Furthermore, by this grid definition specific values for one parameter are evaluated several times (with different values for the other parameters). Depending on the design of the objective function, this can yield some redundant information, which is solved by the Monte-Carlo method. Although not ideal as an optimization tool, grid search can be used to identify the more promising parts of the search domain.

7.2.2. Monte-Carlo Method

The Monte-Carlo method has the power to tackle a multi-dimensional parameter space more efficiently than it can be done with grid search. For the Monte-Carlo method, points in the parameter space are selected randomly. Therefore, implementing constraints to the parameter space obviously requires no effort. This method usually outperform the grid search method, but since it is not target-oriented, getting a good result is rather tedious. Therefore, the two remaining methods are to be preferred.

7.2.3. Genetic Algorithm

In the classical genetic algorithm (GA), all parameters are encoded with a certain number of bits. Typically, the largest binary number (only ones) represents the highest value that this parameter can take and the lowest binary number (only zeros) represents its lowest possible value. It should be noted, that this makes the values that the parameters in the GA can assume discrete. Therefore, it can not be expected to hit a local (or even the global) optimum exactly. Now, one set of parameters is represented by one long bit string containing all the parameters in binary numbers. The GA works with generations. Each generation has a set number of elements (generation size). All elements of a generation have a fitness value that is either known from the previous generation if this element has not been changed, or the fitness function has to be evaluated. With all the fitness values being known, the composition of the next generation is to be determined. For this, several parts can be applied and combined:

- **Elites** are the elements that are transferred to the next generation without any change. This is usually a fixed percentage of the elements with the best fitness value.
- **Children** are elements that are created out of the elements that do not belong to the elites. For this, usually two parents are combined by taking each bit randomly from one of the parents.
- **Immigrants** are new elements that are generated completely randomly.
- **Mutation** affects some of the bits of the children (or children and elites). It randomly toggles a small number of the bits.

All parts can be adjusted in many ways, like the elites ratio, the immigration ratio, the mutation rate, the way children are generated, et cetera. Which settings are beneficial for the optimization depends on the parameters and the objective function. For example the existence of local optima can strongly influence the optimal choice of GA parts. This has to be evaluated for every optimization from scratch. The GA as described here (with binary representation) has been followed up by versions that deal with floating point representations directly.

7.2.4. Particle Swarm Optimization

As the GA, the particle swarm optimization (PSO) uses a certain number of elements that change each generation. Unlike the GA, the parameters are not constrained to discrete values by the representation with binary numbers, but they can take any position in the parameter space. Every particle has a current parameter set (position in parameter space), a velocity (change of position per generation), and a memory containing its best past position and the corresponding fitness value. Every generation, each particle's velocity is changed (the particle is accelerated) towards both, its own best past position and the overall best past position that any particle has found already. These two acceleratiosn are defined by two different constants that are to be chosen for the PSO.

7.2.5. Conclusions

Grid search is useful for visualizing objective functions whose properties are already known, since the order in the data allows for easy plotting. For optimization on the other hand, grid search is to be avoided, since already the (also quite easy to implement) Monte-Carlo method usually outperforms it. The two more advanced methods GA and PSO should be used for global optimization.

7.3. Local Optimization Methods

After a global optimization method has found a point (a set of parameters) that appears to be close to the global optimum, a local optimization method needs to be applied. It should be noted that a local optimizer does not aim to find the global optimum, but merely the local optimum which is *close* to the starting point of the local optimizer. *Close* should not be taken literally. It does not necessarily refer to the one local optimum whose parameters have the smallest Euclidean distance to the starting point. In fact, depending on the local optimizer it can mean different things, the most common of which would be: the one local optimum that is found by always following the steepest descent (or steepest ascent, for maximization problems). This shows that the local optimizer should only be used when one is sure to be close to the global optimum of the problem.

7.3.1. Steepest Descent Method

The steepest descent method requires the objective function to be (analytically or numerically) differentiable. Given one starting point, the gradient is evaluated at this point. Now, the direction of the steepest descent (or ascent, if the optimization is a maximization) is considered. This direction is being followed with falling (increasing for maximization) fitness values until the fitness values start to increase again (decrease for maximization). Then, the gradient is evaluated again and the new line of steepest descent is being followed. For searching the optimum along the line, several options are possible, for example using a simple one dimensional grid search with a carefully chosen step size depending on the application.

7.3.2. Nelder-Mead Method

The Nelder-Mead algorithm is another local optimizer. Unlike the steepest descent method it does not require the availability of the first derivative. In an n-dimensional parameter space, the starting point for this method are $n + 1$ points. As stated in the original proposal from Nelder and Mead [42], it requires all $n + 1$ to be *close enough* to each other, meaning that certain requirements on smoothness can be expected from the fitness function. Then, the point that has the worst fitness value is replaced by a point that has a better fitness value. This is repeated until the fitness values of all points are within a previously defined span. Then the algorithm is terminated and the set of parameters that represent the best fitness value is taken. In the core of the algorithm a decision is made between *reflection*, *expansion*, *contraction* and *shrinking*, which can be seen in Figure 7.3. The most straight-forward choice is *reflection*. This means that the point with the worst fitness value is mirrored at the mean of all the other points (called mirror point here). The procedure that follows depends on the fitness of the mirrored point. If its fitness is better than all of the other fitness values and this seems to hold for more points in this direction, the search area is expanded in this direction (*expansion*). On the other hand, if the mirrored point is in fact better than the unmirrored point (which was the worst of all) but not better than the best, the search volume is not increased but shifted in this direction (*reflection*). Finally, if the mirrored point is not better than the unmirrored point, it means that the search area in this direction is too large. Therefore, if the point between the mean of the other points and the mirrored point has

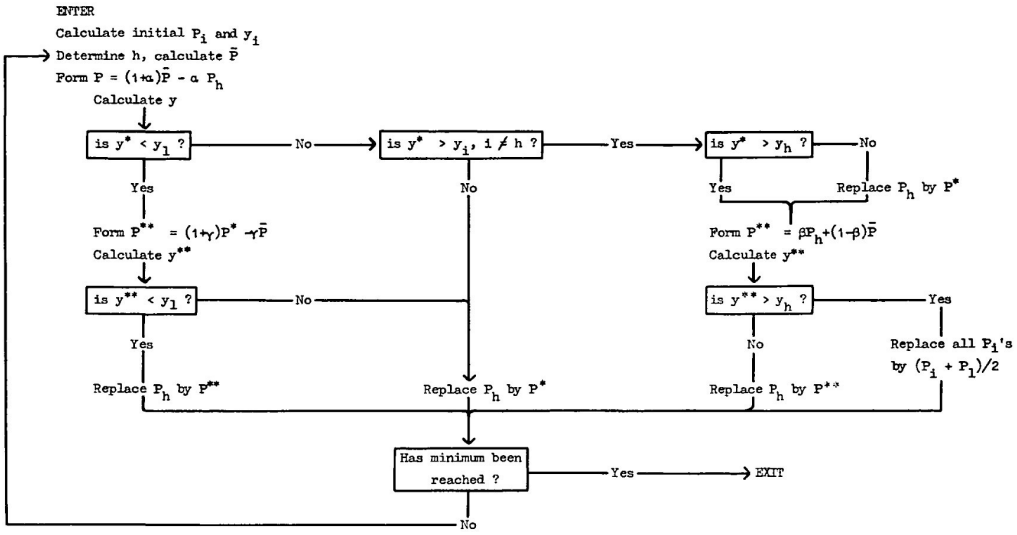

Figure 7.2: Original proposal for the Nelder-Mead algorithm. [42]

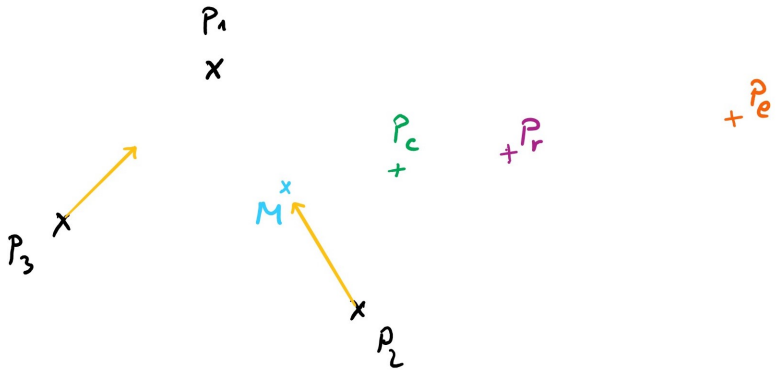

Figure 7.3: Sketch of one Nelder-Mead step in two dimensions. The starting point are the points P_1 to P_3 with P_1 having the best and P_3 having the worst fitness value. Point M (mean of P_1 and P_2) is the mirror point. The mirrored point P_r is P_3 reflected at the mirror M, P_c is a point closer to the mirror and P_e farther from the mirror. Depending on their fitness values, P_3 is replaced by P_r (*reflection*), P_e (*expansion*), or P_c (*contraction*). In the worst case, a *shrinking* takes place, then P_2 and P_3 move towards P_1 (yellow arrows).

a higher fitness than the unmirrored point, this point is taken and thus the search area is decreased (*contraction*). Otherwise, the points seem to be not in a area that has a smooth enough behavior for this algorithm. This does not happen if the starting points had been chosen correctly. In this case, all points are moved towards the best point (*shrinking*). This algorithm is repeated until a termination condition is met.

7.3.3. Conclusions

Since it is not expected that the optimization tasks provide an analytical expression for the first derivative, the steepest descent method will probably be used with approximating the gradient with finite differences. The Nelder-Mead method works independently from derivatives. In case none of these yield a good result, other methods will have to be taken into consideration, of course.

8

Tools

8.1. Tudat and PaGMO

The TU Delft Astrodynamics Toolbox (Tudat) whose documentation can be found in [13], is a tool for astrodynamic simulations. It can help answering astrodynamic problems, finding and optimizing trajectories, incorporating perturbations of all kinds (spherical harmonics gravity, radiation pressure, atmospheric drag, ...), etcetera. It consists of C++ libraries that are publicly available, developed mainly at Delft University of Technology. It can be run with C++ and JSON files and recently also with Python.

In terms of trajectory planning – and designing the trajectory of an asteroid to an Earth-Moon DRO is one possible thesis topic –, Tudat offers all kinds of propagators and integrators and the possibility of defining custom propagators. The latter can be in particular useful when trying to come up with a new set of parameters for DROs. Furthermore, among the state also variational equations can be propagated which enables for example the computation of monodromy matrices and other stability parameters.

Preliminary mission design is enabled by the implemented Lambert targeter, patched-conics multiple-gravity assist, shape-based low thrust models, et cetera. Because of the special properties of DROs that include not knowing which of the primaries should be seen as the central mass in a simulation, the applicability of those methods has yet to be determined.

The Parallel Global Multiobjective Optimizer (PaGMO) [7] is an optimization library that can easily included in Tudat since its language is C++. Besides GA, PSO, Nelder-Mead method, and steepest descent method – which have been mentioned in Chapter 7 – it offers a wide variety of optimization.

The following list aims to give an overview of what functionalities of Tudat are required for the thesis project and to what extent they are already implemented.

Required Elements:	**Availability in Tudat?**
Acceleration Models	Point mass gravity including 3rd body gravity, spherical harmonics gravity, atmospheric drag and lift, solar radiation pressure, and thrust are included. It is not expected that other acceleration models will be needed.
Full Ephemeris	yes, from JPL [25]
Propagator Settings	Cowell, Kepler elements, MEE, and USM are available. Own propagators will have to be implemented.
Integrator Settings	RK4, RKF, ABM, BS, and DOPRI are available. It is not expected that another integrator is needed.
Preliminary mission design	Lambert targeter, patched-conics multiple gravity assist, and shape-based low thrust models are included. It is not expected that other preliminary mission design methods will be needed.
CR3BP	The CR3BP can easily be applied in Tudat.
Optimization Package	PaGMO is a C++ optimization library that can be included in Tudat.

8.2. MATLAB

MATLAB [36], originally *MATrix LABoratories*, is a software created by the company *The MathWorks, Inc.* that aims to offer an easy solution for scientific programming. It can handle matrices, vectors, imaginary numbers, calculations of any kind, etcetera. It can be used in an object-oriented way as well as without the use of objects at all. For the thesis, the main benefit of MATLAB will be the many functionalities regarding plotting that help to present the achieved knowledge in an understandable way.

Furthermore, MATLAB is perfectly able to run simple simulations as finding the initial conditions for DROs or calculating the monodromy matrix of one orbit. More complex tasks as trajectory planning or simulations that include perturbations are left to Tudat which can not only handle perturbations efficiently and with less coding effort, but works more efficiently in general because it is based on C++.

9

Conclusions and Research Questions

In this chapter, overall conclusions are drawn that arise from the finding of the previous chapters. From these conclusions, the research questions will be deduced which finally result in the thesis planning.

9.1. Conclusions

The conclusions can be divided into five topics.

Regarding **modeling of Distant Retrograde Orbits**: There are two modeling techniques that already exist. Firstly, a Fourier series approach that enables calculating position and velocity of a periodic DRO in the CR3BP efficiently. Secondly, a Lindstedt-series approach that accounts for the librating corrections that non-perfect quasi-periodic DROs are facing. This is done with the assumptions of the Hill problem, which include that the secondary and the third body are *close* to each other, which can not be expected to be true in the general case. None of those existing modeling techniques are flexible enough to take (state- and time-dependent) perturbations of any kind into account. Therefore, a new modeling technique for DROs would be beneficial to have.

Regarding **transfers to Distant Retrograde Orbits**: The transfer to DROs can be categorized into three classes. Transfers from the primary to the DRO, transfers from the secondary to the DRO and transfers from a place or orbit that lies outside of the primary-secondary system. While the first two classes have been subject of intensive research already, the transfer from the outside to a Distant Retrograde Orbit has not been analyzed in detail yet. Therefore, this can be considered an interesting research topic for the thesis project. This is relevant for two different cases: capturing an asteroid into an Earth-Moon DRO and inserting a spacecraft into a planet-moon DRO, for example a Jupiter-Europa DRO. These cases are vastly different since the spacecraft can get a significantly larger ΔV caused by propulsion due to its smaller mass. Therefore, those two transfers are to be investigated.

Regarding **propagation and integration**: The usual propagators are the Cowell propagator, which represents the state of an object with three position and three velocity components in a Cartesian coordinate system; the Kepler elements propagator, the MEE propagator and the USM, which represent the state in different modifications of the Kepler elements; and the Encke propagator in which the state is the Cartesian difference between position and velocity of the propagated object and an analytically propagated Kepler orbit. The ones that are closely related to the geometry of Kepler elements (which is the case for all except for the Cowell propagator) are not expected to be of great use when it comes to DROs. Their advantages come into play only for orbits that are similar to Kepler orbits. This is not the case for DROs, since instead of orbiting one main body, two bodies are orbited. Therefore, a short term simulations is likely to be performed with the Cowell propagator, while for long term simulations a derivative of the Encke propagator that uses the Fourier series approximation of DROs instead of Kepler orbits could be tried. In any case, due to no clear preference towards any propagator, the best propagator will always have to be detected in a numerical analysis. Furthermore, this begs for a new set of parameters – that are analytically, unlike the Fourier series approach – suiting to DROs that can

be developed in the thesis project.

Regarding **optimization**: If the number of parameters for the optimization is not too big, a coarse grid can be applied to the parameter space in order to visualize the objective function. However, optimization should not be based on grid search, since this is a highly inefficient method. The optimization should be divided into a global optimization, which aims to get close to the global optimum, and a local optimization which then finds the exact set of parameters that is optimal. For the global optimization, the GA and the PSO are recommended, while for the local optimization the Nelder-Mead method should be used. If the objective function happens to be analytically or numerically differentiable, local optimization can also be performed with the steepest descent method.

Regarding **tools**: *Tudat* is a great publicly available tool that has almost all of the required features itself. A potentially needed own set of parameters can be implemented. Optimization can be done with the library *PaGMO*. Post-processing and plotting will be done with *MATLAB*.

9.2. Research Questions

With the conclusions from the previous section, two main research questions can be identified that can be split into sub-questions. Those two primary questions represent the two options that exist for the thesis. The primary research questions and their respective sub-questions are:

Thesis Topic 1: Can a novel set of elements suit the requirements for both, modeling and propagating Distant Retrograde Orbits?

- Can the Fourier series approach be basis for this new set, for example by considering the difference to it similar to the Encke method?
- Can the elliptical shape of DROs in the Hill problem be exploited to come up with the new set of elements?
- Can the new set of elements help to model and understand Distant Retrograde Orbits better?
- Can the new set of elements help to predict Distant Retrograde Orbits, their long term behavior, and their stability better and more efficiently?
- Does this new set of elements perform better in terms of accuracy and computation time than the existing propagators?
- Does the performance of the new set of elements depend on the mass ratio of the primaries?
- Can complete transfers to DROs be modeled with the new set of elements?

Thesis Topic 2: How would an asteroid be transferred into an Earth-Moon Distant Retrograde Orbit and how can it be used as a space hub?

- What is the optimal DRO for this in terms of stability and accessibility?
- What is the optimal transfer of an asteroid to the DRO in terms of ΔV?
- What is the optimal transfer of an asteroid to the DRO in terms of time of flight?
- How would a transfer from Earth to the asteroid in its Distant Retrograde Orbit work?
- How would rendezvous with this asteroid work?
- How can the space hub be used for interplanetary travel?

9.3. Thesis Planning

For the time planning of the thesis it is crucial to first identify the work packages that will have to be tackled and to know the approximate time that they will take. Therefore, for the two thesis options listed in the previous section, the work is divided into work packages with brief descriptions of how they will look like:

Thesis Topic 1

WP1: Defining sets of elements. Different options for sets of parameters have to be developed in order to obtain five to ten candidates. Most of the parameters should not change a lot during one orbit. Suitable candidates can be found on different ways: By analyzing the shapes of periodic, quasi-periodic, and period-3 DROs and investigating possibles regularities. The

proposed sets of parameters can be both, two- and three-dimensional.
Expected work time including reporting and buffer: 2.5 weeks.

WP2: **Implementation in Tudat**. In order to evaluate and apply the candidates, they have to be implemented in Tudat. This step requires the author to get familiar with the way that propagators are implemented in Tudat first. The implementation itself is expected to be straight forward.
Expected work time including reporting and buffer: 2.5 weeks.

WP3: **Verification and performance evaluation in CR3BP**. To get a first idea of how the new sets of elements work, they are applied in the CR3BP with different mass ratios μ. As a verification, they should yield the same results as the corresponding initial conditions yield with an already existing propagator, for example *Cowell*. The performance should be evaluated in terms of accuracy and computational effort while representing the parameters with varying numbers of digits.
Expected work time including reporting and buffer: 2 weeks.

WP4: **Verification and performance evaluation with full ephemeris**. The same should be applied to various full ephemeris examples in different two-body systems. Consequently, one of the candidates is selected to be regarded for the remaining work packages.
Expected work time including reporting and buffer: 3 weeks.

WP5: **Modeling of DROs with new elements**. The best possible way of modeling periodic or quasi-periodic DROs with the new parameters should be found. This can for example be done with a Fourier analysis as described in Section 4.1, or with a novel approach.
Expected work time including reporting and buffer: 8 weeks.

WP6: **Stability analysis with new elements**. To confirm the proper work of the new set of elements, a stability analysis including the evaluation of the monodromy matrix should be executed.
Expected work time including reporting and buffer: 2 weeks.

WP7: **Transfer with new elements**. It should be assessed, if the new elements make transfer to DROs easier to simulate and if mission planning is simplified. This shall be done with the example of a transfer from Earth to an Earth-Moon DRO.
Expected work time including reporting and buffer: 7 weeks.

WP8: **Final reporting, buffer, and thesis defense**.
Expected work time including reporting and buffer: 3 weeks. Total: 30 weeks.

Thesis Topic 2

WP1: **Selection of an asteroid**. One or multiple suitable asteroids that have a low enough mass to make thrust initiated orbital changes possible and whose orbits are close to the Earth's orbit should be selected.
Expected work time including reporting and buffer: 1 week.

WP2: **Selection of Earth-Moon DRO specifics**. As a target orbit for the asteroid, a suitable Earth-Moon DRO shall be selected. It should be stable for more than one millennium and have a similar energy as Sun-orbiting, near-Earth asteroids in order to make the transfer less ΔV-costly.
Expected work time including reporting and buffer: 4 weeks.

WP3: **Deciding for propagator/integrator settings**. This will be done by comparing different propagator and integrator settings to a prior created benchmark solution and selecting the best performing settings.
Expected work time including reporting and buffer: 2.5 weeks.

WP4: **Including PaGMO**. The PaGMO library needs to be included in Tudat and understood by the author in order to be usable.
Expected work time including reporting and buffer: 1.5 weeks.

WP5: **Optimizing transfer trajectory for asteroid**. A (probably low-thrust) transfer into the Earth-Moon DRO should be found and optimized. This is done with the use of PaGMO.
Expected work time including reporting and buffer: 7 weeks.

WP6: **Optimizing transfers from Earth to asteroid**. Similarly, in order to use the asteroid as a space hub, transfers from Earth to the Earth-Moon DRO have to be planned and optimized in terms of ΔV and time of flight.
Expected work time including reporting and buffer: 7 weeks.

WP7: **Feasibility study for interplanetary transfer through space hub DRO**. Transfers from the

DRO to other planets should be found. Then, the asteroid can serve as a space hub and possibly refill station, opening the solar system for future space exploration and colonization.
Expected work time including reporting and buffer: 4 weeks.

WP8: Final reporting, buffer, and thesis defense.
Expected work time including reporting and buffer: 3 weeks. Total: 30 weeks.

Bibliography

[1] R. H. Battin. *An introduction to the mathematics and methods of astrodynamics*. AIAA education series. American Institute of Aeronautics and Astronautics, Reston, VA, rev. ed. edition, 1999. ISBN 978-1-56347-342-5.

[2] D. Benest. Effects of the Mass Ratio on the Existence of Retrograde Satellites in the Circular Plane Restricted Problem. *Astronomy and Astrophysics*, 32:39, April 1974. ISSN 0004-6361. URL http://adsabs.harvard.edu/abs/1974A%26A....32...39B.

[3] D. Benest. Libration effects for retrograde satellites in the restricted three-body problem. *Celestial mechanics*, 13(2):203–215, March 1976. ISSN 1572-9478. doi: 10.1007/BF01232724. URL https://doi.org/10.1007/BF01232724.

[4] C. J. Bezrouk and J. S. Parker. Long Duration Stability of Distant Retrograde Orbits. In *AIAA/AAS Astrodynamics Specialist Conference*, San Diego, CA, August 2014. American Institute of Aeronautics and Astronautics. ISBN 978-1-62410-308-7. doi: 10.2514/6.2014-4424. URL http://arc.aiaa.org/doi/10.2514/6.2014-4424.

[5] C. J. Bezrouk and J. S. Parker. Long term evolution of distant retrograde orbits in the Earth-Moon system. *Astrophysics and Space Science*, 362(9):176, August 2017. ISSN 1572-946X. doi: 10.1007/s10509-017-3158-0. URL https://doi.org/10.1007/s10509-017-3158-0.

[6] C. J. Bezrouk and J. S. Parker. Ballistic capture into distant retrograde orbits around Phobos: an approach to entering orbit around Phobos without a critical maneuver near the moon. *Celestial Mechanics and Dynamical Astronomy*, 130(2):10, January 2018. ISSN 1572-9478. doi: 10.1007/s10569-017-9798-0. URL https://doi.org/10.1007/s10569-017-9798-0.

[7] Francesco Biscani and Dario Izzo. A parallel global multiobjective framework for optimization: pagmo. *Journal of Open Source Software*, 5(53):2338, September 2020. ISSN 2475-9066. doi: 10.21105/joss.02338. URL https://joss.theoj.org/papers/10.21105/joss.02338.

[8] D. Boccaletti and G. Pucacco. *Theory of orbits*. Astronomy and astrophysics library. Springer, Berlin; New York, corr. 3rd print edition, 2004. ISBN 978-3-540-58963-1.

[9] R. L. Burden and J. D. Faires. *Numerical analysis*. Brooks/Cole, Cengage Learning, Boston, MA, 9th ed edition, 2011. ISBN 978-0-538-73351-9. OCLC: ocn496962633.

[10] L. R. Capdevila and K. C. Howell. A transfer network linking Earth, Moon, and the triangular libration point regions in the Earth-Moon system. *Advances in Space Research*, 62(7):1826–1852, October 2018. ISSN 0273-1177. doi: 10.1016/j.asr.2018.06.045. URL http://www.sciencedirect.com/science/article/pii/S027311771830543X.

[11] L. R. Capdevila, D. Guzzetti, and K. C. Howell. Various Transfer Options From Earth into Distant Retrograde Orbits in the Vicinity of the Moon. In *Spaceflight Mechanics 2014: Advances in the Astronautical Sciences*, volume 152, page 20. Univelt, San Diego, CA. URL https://pdfs.semanticscholar.org/3129/a7ee306b15c600f6aa647decdae5375649ad.pdf. Accessed: 26-11-2020.

[12] W. H. Clohessy and R. S. Wiltshire. Terminal Guidance System for Satellite Rendezvous. *Journal of the Aerospace Sciences*, 27(9):653–658, September 1960. ISSN 1936-9999. doi: 10.2514/8.8704. URL https://arc.aiaa.org/doi/10.2514/8.8704.

[13] Delft University of Technology. TU Delft Astrodynamics Toolbox (Tudat), 2018. URL https://tudat.tudelft.nl/. Accessed: 13-11-2020.

[14] J. Demeyer and P. Gurfil. Transfer to Distant Retrograde Orbits Using Manifold Theory. *Journal of Guidance, Control, and Dynamics*, 30(5):1261–1267, 2007. doi: 10.2514/1.24960. URL https://doi.org/10.2514/1.24960.

[15] J. Demeyer, P. Gurfil, and E. Belbruno. Transfer to Small Distant Retrograde Orbits. *AIP Conference Proceedings*, 886(1):20–31, February 2007. ISSN 0094-243X. doi: 10.1063/1.2710041. URL https://aip.scitation.org/doi/abs/10.1063/1.2710041.

[16] D. Dirkx and K. Cowan. AE4868 – Numerical Astrodynamics – Numerical Integration, December 2018. Delft University of Technology, Delft, The Netherlands.

[17] D. Dirkx and K. Cowan. AE4868 – Numerical Astrodynamics – Acceleration Models, November 2019. Delft University of Technology, Delft, The Netherlands.

[18] D. Dirkx and E. Mooij. AE4866 – Propagation and Optimization – Formulation of Equations of Motion, February 2019. Delft University of Technology, Delft, The Netherlands.

[19] L. N. Hand and J. D. Finch. *Analytical mechanics*. Cambridge University Press, Cambridge; New York, 1998. ISBN 978-0-521-57572-0.

[20] M. Henon. Numerical Exploration of the Restriced Problem. V. Hill's Case: Periodic Orbits and Their Stability. *Astron. & Astrophys.*, 1:223–238, November 1968. URL https://ui.adsabs.harvard.edu/abs/1969A%26A.....1..223H/abstract. Accessed: 05-10-2020.

[21] M. Henon. Numerical Exploration of the Restriced Problem. VI. Hill's Case: Non-Periodic Orbits. *Astron. & Astrophys.*, 9:24–36, May 1970. URL https://ui.adsabs.harvard.edu/abs/1970A%26A.....9...24H/abstract. Accessed: 05-10-2020.

[22] M. Henon and J.-M. Petit. Series expansions for encounter-type solutions of Hill's problem. *Celestial Mechanics*, 38(1):67–100, January 1986. ISSN 0008-8174, 1572-9478. doi: 10.1007/BF01234287. URL http://link.springer.com/10.1007/BF01234287.

[23] G. W. Hill. Researches in the Lunar Theory. *American Journal of Mathematics*, 1(1):5–26, 1878. ISSN 0002-9327. doi: 10.2307/2369430. URL https://www.jstor.org/stable/2369430. Publisher: Johns Hopkins University Press.

[24] A. N. Hirani and R. P. Russell. Approximations of distant retrograde orbits for mission design. January 2006. URL https://trs.jpl.nasa.gov/handle/2014/38896.

[25] Jet Propulsion Laboratory. JPL Planetary and Lunar Ephemerides. URL https://ssd.jpl.nasa.gov/?planet_eph_export. Accessed: 26-11-2020.

[26] M. Kimura, M. Kawamura, and K. Yamada. Analytical expression for distant retrograde orbits around a small natural satellite. *Advances in Space Research*, 63(3):1336–1346, February 2019. ISSN 02731177. doi: 10.1016/j.asr.2018.10.026. URL https://linkinghub.elsevier.com/retrieve/pii/S0273117718307956.

[27] W. Kutta. *Beitrag zur näherungsweisen Integration totaler Differentialgleichungen*. Teubner, 1901.

[28] J. L. Lagrange. *Mécanique analytique*. Ve Courcier, 1811.

[29] J. L. Lagrange. *Mécanique analytique*. Mallet-Bachelier, 1815.

[30] T. Lam and G. J. Whiffen. Exploration of Distant Retrograde Orbits Around Europa (AAS 05-110). *Advances in the Astronautical Sciences*, 120, January 2005. URL https://trs.jpl.nasa.gov/bitstream/handle/2014/37526/05-0195.pdf. In: Vallado DA, Gabor MJ, Desai PN (eds) AAS/AIAA Spaceflight Mechanics Meeting 2005, American Astronautical Society, Univelt, Inc., USA.

[31] M. Langelaar. ME46060 – Engineering Optimization – Lecture 2, 2020. Delft University of Technology, Delft, The Netherlands.

[32] M. Lara. Higher order analytical solution to the distant retrograde orbits problem. Bremen, Germany, October 2018. International Astronautical Federation (IAF).

[33] M. Lara. Nonlinear librations of distant retrograde orbits: a perturbative approach—the Hill problem case. *Nonlinear Dynamics*, 93(4):2019–2038, September 2018. ISSN 1573-269X. doi: 10.1007/s11071-018-4304-0. URL https://doi.org/10.1007/s11071-018-4304-0.

[34] M. Lara. Design of distant retrograde orbits based on a higher order analytical solutiont. *Acta Astronautica*, 161:562–578, August 2019. ISSN 0094-5765. doi: 10.1016/j.actaastro.2019.01.039. URL http://www.sciencedirect.com/science/article/pii/S0094576518319155.

[35] M. Lara, R. Russell, and B. Villac. Classification of the Distant Stability Regions at Europa. *Journal of Guidance, Control, and Dynamics*, 30(2):409–418, 2007. doi: 10.2514/1.22372. URL https://doi.org/10.2514/1.22372.

[36] MathWorks Inc. MATLAB, 2020. URL https://nl.mathworks.com/products/matlab.html. Accessed: 13-11-2020.

[37] X. Ming and X. Shijie. Exploration of distant retrograde orbits around Moon. *Acta Astronautica*, 65(5):853–860, September 2009. ISSN 0094-5765. doi: 10.1016/j.actaastro.2009.03.026. URL http://www.sciencedirect.com/science/article/pii/S0094576509001404.

[38] T. Minghu, Z. Ke, L. Meibo, and X. Chao. Transfer to long term distant retrograde orbits around the Moon. *Acta Astronautica*, 98:50–63, May 2014. ISSN 0094-5765. doi: 10.1016/j.actaastro.2014.01.016. URL http://www.sciencedirect.com/science/article/pii/S0094576514000290.

[39] B. K. Muirhead and J. R. Brophy. Asteroid Redirect Robotic Mission feasibility study. In *2014 IEEE Aerospace Conference*, pages 1–14, March 2014. doi: 10.1109/AERO.2014.6836358. ISSN: 1095-323X.

[40] N. Murakami and K. Yamanaka. Trajectory design for rendezvous in lunar Distant Retrograde Orbit. In *2015 IEEE Aerospace Conference*, pages 1–13, March 2015. doi: 10.1109/AERO.2015.7119023. ISSN: 1095-323X.

[41] James A. Murdock. *Perturbations: Theory and Methods*. Society for Industrial and Applied Mathematics, January 1999. ISBN 978-0-89871-443-2 978-1-61197-109-5. doi: 10.1137/1.9781611971095. URL http://epubs.siam.org/doi/book/10.1137/1.9781611971095.

[42] J. A. Nelder and R. Mead. A Simplex Method for Function Minimization. *The Computer Journal*, 7(4):308–313, January 1965. ISSN 0010-4620. doi: 10.1093/comjnl/7.4.308. URL https://academic.oup.com/comjnl/article/7/4/308/354237. Publisher: Oxford Academic.

[43] I. Newton. *The Mathematical Principles of Natural Philosophy*. 1729.

[44] C. A. Ocampo and G. W. Rosborough. Transfer trajectories for distant retrograde orbiters of the Earth. *NASA STI/Recon Technical Report A*, 95:1177–1200, 1993. URL http://adsabs.harvard.edu/abs/1993STIA...95814180. Accessed: 27-10-2020.

[45] J. S. Parker and R. L. Anderson. *Low-Eenergy Lunar Trajectory Design*. John Wiley & Sons, Inc., Hoboken, NJ, USA, June 2014. ISBN 978-1-118-85506-5 978-1-118-85387-0. doi: 10.1002/9781118855065. URL http://doi.wiley.com/10.1002/9781118855065.

[46] P. Pires and O. C. Winter. Location and stability of distant retrograde orbits around the Moon. *Monthly Notices of the Royal Astronomical Society*, 494(2):2727–2735, May 2020. ISSN 0035-8711, 1365-2966. doi: 10.1093/mnras/staa887. URL https://academic.oup.com/mnras/article/494/2/2727/5817352.

[47] C. Runge. Ueber die numerische Aufloesung von Differentialgleichungen. June 1895. doi: 10.1007/bf01446807. URL https://zenodo.org/record/2178704.

[48] D. J. Scheeres. *Orbital motion in strongly perturbed environments: applications to asteroid, comet and planetary satellite orbiters*. Springer-Praxis books in astronautical engineering. Springer ; Published in association with Praxis Publishing, Heidelberg ; New York : Chichester, UK, 2012. ISBN 978-3-642-03255-4. OCLC: ocn428029964.

[49] C. J. Scott. Transfer and Capture into Distant Retrograde Orbits. January 2010. URL https://etda.libraries.psu.edu/catalog/10471. Accessed: 15-09-2020.

[50] C. J. Scott and D. B. Spencer. Calculating Transfer Families to Periodic Distant Retrograde Orbits Using Differential Correction. *Journal of Guidance, Control, and Dynamics*, 33(5):1592–1605, 2010. doi: 10.2514/1.47791. URL https://doi.org/10.2514/1.47791.

[51] C. J. Scott and D. B. Spencer. Transfers to Sticky Distant Retrograde Orbits. *Journal of Guidance, Control, and Dynamics*, 33(6):1940–1946, 2010. doi: 10.2514/1.47792. URL https://doi.org/10.2514/1.47792.

[52] V. G. Szebehely. *Theory of Orbits, The Restricted Problem of Three Bodies*. Academic Press Inc., Yale University, New Haven, Connecticut, 1967.

[53] The University of Texas at Austin. Normalized Gravity Coefficients. URL http://www.csr.utexas.edu/publications/statod/TabD.3.new.txt. Accessed: 18-11-2020.

[54] G. Turner. Results of long-duration simulation of Distant Retrograde Orbits. *Aerospace*, 3(4), 2016. doi: 10.3390/aerospace3040037.

[55] V. Vittaldev, E. Mooij, and M. C. Naeije. Unified State Model theory and application in astrodynamics. *Celestial mechanics and dynamical astronomics, 112(3)2012*, 2012. ISSN 0923-2958. doi: 10.1007/s10569-011-9396-5. URL https://repository.tudelft.nl/islandora/object/uuid%3A2caeefbc-ab6a-44d6-888e-2e8b82a2ae8c. Publisher: Springer.

[56] K. F. Wakker. *Fundamentals of Astrodynamics*. Institutional Repository, Library, Delft University of Technology, Delft, The Netherlands, January 2015. ISBN 978-94-6186-419-2. URL http://resolver.tudelft.nl/uuid:3fc91471-8e47-4215-af43-718740e6694e.

[57] C. M. Welch, J Parker, S., and C. Buxton. Mission Considerations for Transfers to a Distant Retrograde Orbit. *The Journal of the Astronautical Sciences*, 62(2):101–124, June 2015. ISSN 2195-0571. doi: 10.1007/s40295-015-0039-z. URL https://doi.org/10.1007/s40295-015-0039-z.

[58] R. Zhang, Y. Wang, H. Zhang, and C. Zhang. Transfers from distant retrograde orbits to low lunar orbits. *Celestial Mechanics and Dynamical Astronomy*, 132(8):41, August 2020. ISSN 1572-9478. doi: 10.1007/s10569-020-09982-4. URL https://doi.org/10.1007/s10569-020-09982-4.